JOURNAL OF GUIDANCE, CONTROL, AND DYNAMICS
Vol. 31, No. 3, May–June 2008

Vision-Based Target Geolocation Using Micro Air Vehicles

Meir Pachter*
U.S. Air Force Institute of Technology, Wright–Patterson Air Force Base, Ohio 45433
and
N. Ceccarelli† and P. R. Chandler‡
U.S. Air Force Research Laboratory, Wright–Patterson Air Force Base, Ohio 45433

DOI: 10.2514/1.31896

A method for determining the location of a stationary ground target when imaged from the air using a camera-equipped micro air vehicle is developed. The ground object's elevation is assumed known. Rather than a "one-shot" affair, multiple bearing measurements of the ground object taken as the aircraft flies around the target are used. This makes it possible for the adverse effects of both the random measurement errors and the systematic measurement errors (i.e., attitude sensors' biases) to be mitigated. The main result of this paper is that when bearing measurements of a target are taken over time, the target's position and the micro air vehicle's systematic attitude-measurement errors can be jointly estimated using linear regression. As a result, the target is accurately geolocated and the attitude sensors are calibrated. If only one snap bearing measurement of the target can be taken, the attitude sensors will be calibrated before arrival at the target area using an initial point. The technique was successfully tested on actual flight data collected during multiple micro air vehicle operations for cooperative geolocation of unknown targets.

Nomenclature

C	=	direction cosines matrix
f	=	focal length of the camera lens
f_{GPS}	=	data acquisition frequency for the global positioning system receiver
R	=	position vector
T_{dwell}	=	dwell time of the target inside the camera's footprint
(x, y, z)	=	Cartesian coordinates of the air vehicle
ζ, ξ	=	line-of-sight angles
ρ	=	turn radius
(ψ, θ, ϕ)	=	Euler angles of the air vehicle

Subscripts

b	=	body frame
c	=	calculated
f	=	focal plane
k	=	sample
m	=	measured variable
n	=	navigation frame
P	=	ground object/target

Superscripts

b	=	body frame
n	=	navigation frame

I. Introduction

IN SUPPORT of the current Cooperative Operation in Urban Terrain program [1], a micro air vehicle (MAV)-based intelligence, surveillance, and reconnaissance [2] mission is considered. Recent works [3] and reference therein have provided successful examples of vision-aided autonomous aerial operations. In this paper, it is envisaged that camera-equipped MAVs are used, and a method for determining the location of a fixed ground object when imaged from air vehicles is developed. The pixel location of the object in the image, the position and attitude of the air vehicles, the camera's pose angles, and knowledge of the terrain elevation are used to geolocate the object. Previous target localization work using a camera-equipped MAV is reported in [4], and geolocation using long-endurance unmanned aerial vehicles has been reported in [5]. In this paper, rather than a "one-shot" affair, multiple bearing measurements of the ground object taken as the aircraft flies over the object/target are used. We assume that the target is identified by a human operator and is subsequently tracked using a feature-tracking [6] algorithm; alternatively, the target could be manually tracked by the human operator. Taking the target's bearing measurements over time ensures that adverse effects of both the random measurement errors and the systematic measurement errors (i.e., attitude sensors' biases) are mitigated. Although vision-based navigation [7–9] has been previously studied for different aerial platforms, the main result of this paper is that the target's position and the MAV's systematic attitude-measurement errors can be jointly estimated using measurements taken over time and linear regression [10]. As a result, the target is accurately geolocated. We emphasize that this is in large part due to the action of the automatic feature-tracking algorithm [6], which makes it possible to autonomously track the target designated by the human operator. The feature-tracking algorithm [6] has a good track record: it has successfully been employed in an integrated inertial and optical navigation system [11] and has been proved in simulations, in experiments with ground vehicles, and in flight test. In this work, it is assumed that an efficient autonomous feature-tracking algorithm is available and the emphasis is on the development of the target geolocation algorithm and the estimation of the microelectromechanical system's gyro biases. Finally, the herein developed theory also applies when the target is being manually tracked by an operator. Preliminary results have been presented in [12,13].

The main novelty of the present paper is the realization that the air vehicle's attitude–heading reference system (AHRS) errors can be estimated and are obtained as a byproduct of the developed optical geolocation method; that is, the biases of the positional gyros are estimated. Particular attention is given to the difficult-to-measure heading angle caused by the significant heading measurement error

Presented as Paper 6863 at the AIAA Guidance, Navigation, and Control Conference and Exhibit, Hilton Head, SC, 20–23 August 2007; received 1 May 2007; revision received 31 July 2007; accepted for publication 21 September 2007.

*Professor, Department of Electrical and Computer Engineering.
†National Research Council Fellow.
‡Project Lead, Air Vehicles Directorate.

(i.e., a constant bias of ∼40 deg). The assumption of an unknown but constant bias is justified by the short tracking window ∼2 s, as is the case when the MAVs fly over a target. In addition, the novel geolocation technique, which uses vision, renders the difficult-to-estimate wind vector unnecessary.

Strictly speaking, the AHRS's attitude-measurement error, averaged over the short measurement interval, is acknowledged and is estimated. Thus, whereas the ground-object positioning accuracy achieved when one target bearing is taken is generally poor, due primarily to the low quality of the inertial measurement unit (IMU) onboard MAVs, the novel geolocation method developed in this paper yields a much-enhanced target localization accuracy. Moreover, the biases of the "positional gyros" can be estimated before arriving at the target: a short time before overflying the target, an arbitrary chosen initial point (IP) is tracked for the sole purpose of calibrating the AHRS. This is similar to the operational practice of the inertial navigation system (INS) updating before a bombing run, except that now it is not essential for the coordinates of the IP to be known. We are not interested in the IP's coordinates but, rather, in the biases in the MAV's Euler angles' measurements. Having an estimate of the MAV's attitude-measurement error is then conducive to accurate geolocation from a one-shot target-bearing measurement.

The paper is organized as follows. In Sec. II, the geometry of vision-based geolocation is discussed. The linear regression-based geolocation algorithm is developed in Sec. III. Estimates of the MAV's systematic attitude-measurement errors (i.e., the positional-gyro biases) are also obtained. Furthermore, the predicted covariances of the target's position and the positional gyro's bias estimation errors are provided. In Sec. IV, we give an iterative algorithm for the estimation of large positional-gyro biases, which is based on the linear regression algorithm developed in Sec. III. First, the important special case of a flyover of the target, which reduces the problem to 2-D geometry, is analyzed in detail in Sec. V, whereas the derivation of the regression algorithm is reported in Appendix A. The three-dimensional geometry is analyzed in detail in Sec. VI, in which special attention is given to the estimation of the large yaw-angle measurement bias. The results of simulations performed to validate the performance of the novel geolocation algorithm are presented in Sec. VII. The detailed mathematical derivation is reported in Appendix B. Special attention to geolocation using a single, one-shot, target-bearing measurement is given in Sec. VIII. Results obtained from actual flight data relative to multiple MAVs operations are presented in Sec. IX. Extensions of the developed theory are discussed in Sec. X, followed by concluding remarks in Sec. XI.

II. Geometry

The human operator identifies/detects the ground object of interest and an image processing algorithm extracts the line-of-sight (LOS) direction (see, for example, [6]). Henceforth, the image processing algorithm autonomously tracks the designated feature in the image; alternatively, the target could be manually tracked by the human operator. Thus, bearings-only measurements of the ground object taken over time are obtained. The measurement equation for the vision-based geolocation method flows from the geometry of the measurement arrangement.

The aircraft and the ground-object/feature P are shown in Fig. 1. Without loss of generality, assume the camera and MAV's body axes frames are aligned and collocated. Hence, we exclusively refer to the body b frame. The following holds:

$$R_P = R + R_{\mathrm{LOS}}$$

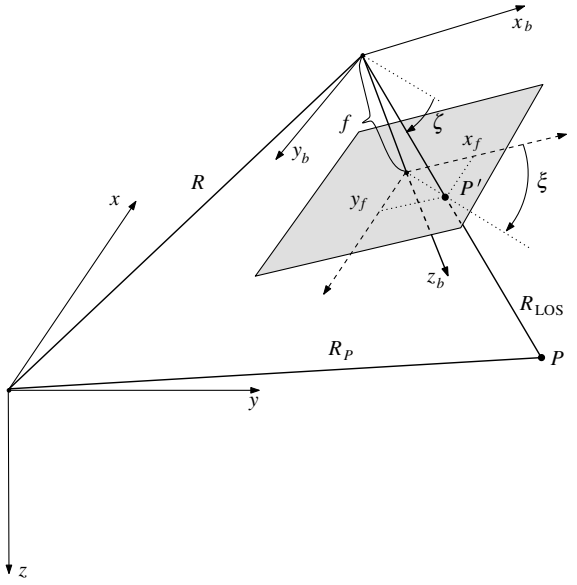

Fig. 1 Line of sight.

and hence

$$R_P^{(n)} = R^{(n)} + C_b^n \cdot R_{\mathrm{LOS}}^{(b)} \tag{1}$$

The measurements x_f and y_f are the coordinates of the image of the ground object P in the camera's focal plane (see Fig. 1, in which the navigation frame and the body frame are shown). The target's image P' is recorded in the image plane. The navigation frame n is attached to the flat and nonrotating Earth. The flat and nonrotating Earth assumption is justified in view of the short range of the MAV operations under consideration.

From Fig. 1,

$$\frac{1}{\sqrt{x_f^2 + y_f^2 + f^2}} \begin{pmatrix} x_f \\ y_f \\ f \end{pmatrix} = \frac{1}{|R_{\mathrm{LOS}}|} R_{\mathrm{LOS}}^{(b)} \tag{2}$$

Combining Eqs. (1) and (2) yields

$$\begin{pmatrix} x \\ y \\ z \end{pmatrix} = \begin{pmatrix} x_P \\ y_P \\ z_P \end{pmatrix} - \frac{|R_{\mathrm{LOS}}|}{\sqrt{x_f^2 + y_f^2 + f^2}} C_b^n \begin{pmatrix} x_f \\ y_f \\ f \end{pmatrix} \tag{3}$$

The navigation state $(x, y, z, \psi, \theta, \phi)^T$ is provided by the onboard global positioning system (GPS) receiver and the AHRS; the MAV's Euler angles feature in the direction cosines matrix (DCM) $C_b^n = C_b^n(\psi, \theta, \phi)$; that is,

$$C_b^n = \begin{bmatrix} \cos\psi\cos\theta & \cos\psi\sin\theta\sin\phi - \sin\psi\cos\phi & \sin\psi\sin\phi + \cos\psi\sin\theta\cos\phi \\ \sin\psi\cos\theta & \cos\psi\cos\phi + \sin\psi\sin\theta\sin\phi & \sin\psi\sin\theta\cos\phi - \cos\psi\sin\phi \\ -\sin\theta & \cos\theta\sin\phi & \cos\theta\cos\phi \end{bmatrix}$$

Equation (3) has the strength of two equations in the six variables that comprise the navigation state. The third equation in Eq. (3) is

$$z_P - z = \frac{|R_{\mathrm{LOS}}|}{\sqrt{x_f^2 + y_f^2 + f^2}} \cdot (0, 0, 1) C_b^n \begin{pmatrix} x_f \\ y_f \\ f \end{pmatrix}$$

and thus,

$$\frac{|R_{\text{LOS}}|}{\sqrt{x_f^2+y_f^2+f^2}}=\frac{z_P-z}{(0,0,1)C_b^n\begin{pmatrix}x_f\\y_f\\f\end{pmatrix}}$$

Inserting this expression into the first two equations in Eq. (3) yields the two equations, referred to as the main equation:

$$\begin{pmatrix}x_P\\y_P\end{pmatrix}=\begin{pmatrix}x\\y\end{pmatrix}+(z_P-z)\frac{1}{(0,0,1)C_b^n\begin{pmatrix}x_f\\y_f\\f\end{pmatrix}}\begin{bmatrix}1&0&0\\0&1&0\end{bmatrix}C_b^n\begin{pmatrix}x_f\\y_f\\f\end{pmatrix} \tag{4}$$

The main equation ties together the MAV's state, the tracked ground object's position, and the measurements.

III. Linear Regression

We estimate the parameter

$$\theta=[\theta_1,\theta_2]^T$$

where

$$\theta_1=[x_P,y_P]^T$$

is the position of the ground object and

$$\theta_2=[\overline{\delta\alpha},\overline{\delta\beta},\overline{\delta\gamma}]^T$$

which quantifies a small-angle rotation misalignment, is the bias error in the attitude measurement provided by the MAV's AHRS. We note that these, however, are not the biases in the Euler angles (see Sec. III.A).

The measured variables are

$$y_1=[x,y,z,x_f,y_f]^T$$

and the DCM

$$C_b^n=C_b^n(\psi,\theta,\phi)$$

The position (x,y,z) of the MAV is provided by the GPS receiver onboard the MAV and (x_f,y_f) are the coordinates of the image of the ground objects in the focal plane of the camera carried by the MAV. The MAV's (3, 2, 1) Euler angles (ψ,θ,ϕ) (i.e., the DCM C_b^n) is provided by the MAV's AHRS. Thus, the measurement equation has the general form

$$\theta_1=f(y_1,C_b^n) \tag{5}$$

where the nonlinear function f is specified by the RHS of Eq. (4).

The actual measurements are

$$z_1=y_1+v_1,\qquad v_1\sim\mathbf{N}(0,R_1) \tag{6}$$

and the strapdown INS/AHRS calculated DCM is

$$\begin{aligned}C_{b_c}^n&=C_b^n+\delta C_b^n=C_b^n+\delta C_b^n\left(\theta_2+v_2;C_b^n\right)\\&\approx C_b^n+\delta C_b^n\left(\theta_2+v_2;C_{b_c}^n\right)\\&=C_b^n+\delta C_b^n(\theta_2+v_2),\qquad v_2\sim\mathbf{N}(0,R_2)\end{aligned} \tag{7}$$

where the Gaussian measurement noise covariances R_1 and R_2 are 5×5 and 3×3 real symmetric positive-definite matrices, respectively. We shall assume that R_1 is a diagonal matrix and $R_2=\sigma^2I_3$. Inserting Eqs. (6) and (7) into the measurement equation (5), we obtain the nonlinear measurement equation:

$$\theta_1=f\left[z_1-v_1,C_{b_c}^n-\delta C_b^n(\theta_2+v_2)\right] \tag{8}$$

As will become apparent, the attitude-measurement error δC_b^n is a linear function of θ_2+v_2 and, moreover, is homogeneous in θ_2+v_2 [i.e., $\delta C_b^n(0)=0$]. Assume the random Gaussian measurement errors v_1 and v_2 are small as is the systematic attitude-measurement error; that is, the bias θ_2, is small. Using Taylor's theorem then gives

$$\begin{aligned}f\left(z_1-v_1,C_{b_c}^n-\delta C_b^n\right)&\approx f\left(z_1,C_{b_c}^n\right)\\&-\left.\frac{\partial f}{\partial y_1}\right|_{z_1,C_{b_c}^n}\cdot v_1-\left.\frac{\partial f}{\partial\theta_2}\right|_{z_1,C_{b_c}^n}\cdot v_2-\left.\frac{\partial f}{\partial\theta_2}\right|_{z_1,C_{b_c}^n}\cdot\theta_2\end{aligned} \tag{9}$$

and combining Eqs. (8) and (9) yields the linearized measurement equation

$$f(z_1,C_{b_c}^n)\approx\theta_1+\left.\frac{\partial f}{\partial\theta_2}\right|_{z_1,C_{b_c}^n}\cdot\theta_2+\left.\frac{\partial f}{\partial y_1}\right|_{z_1,C_{b_c}^n}\cdot v_1+\left.\frac{\partial f}{\partial\theta_2}\right|_{z_1,C_{b_c}^n}\cdot v_2 \tag{10}$$

Suppose that $N(\geq2)$ bearings are taken at the discrete time instants $k=1,\ldots,N$ and the measurements

$$\left(z_{1_1},C_{b_{c_1}}^n\right),\ldots,\left(z_{1_k},C_{b_{c_k}}^n\right),\ldots,\left(z_{1_N},C_{b_{c_N}}^n\right)$$

are accumulated. Using Eq. (10), one generates the linear regression in the parameter $\theta\in R^5$:

$$\begin{pmatrix}f(z_{1_1},C_{b_{c_1}}^n)\\\vdots\\f(z_{1_N},C_{b_{c_N}}^n)\end{pmatrix}=\begin{bmatrix}I_2,&\left.\frac{\partial f}{\partial\theta_2}\right|_{z_{1_1},C_{b_{c_1}}^n}\\\vdots&\vdots\\I_2,&\left.\frac{\partial f}{\partial\theta_2}\right|_{z_{1_N},C_{b_{c_N}}^n}\end{bmatrix}\theta+V \tag{11}$$

The equation error

$$V\sim\mathbf{N}(0,R)$$

and its covariance

$$\begin{aligned}R=\operatorname{diag}\Bigg(\Bigg\{&\left(\left.\frac{\partial f}{\partial y_1}\right|_{z_{1_k},C_{b_{c_k}}^n}\right)R_1\left(\left.\frac{\partial f}{\partial y_1}\right|_{z_{1_k},C_{b_{c_k}}^n}\right)^T\\&+\left(\left.\frac{\partial f}{\partial\theta_2}\right|_{z_{1_k},C_{b_{c_k}}^n}\right)R_2\left(\left.\frac{\partial f}{\partial\theta_2}\right|_{z_{1_k},C_{b_{c_k}}^n}\right)^T\Bigg\}_{k=1}^N\Bigg)\end{aligned}$$

that is,

$$\begin{aligned}R=\operatorname{diag}\Bigg(\Bigg\{&\left(\left.\frac{\partial f}{\partial y_1}\right|_{z_{1_k},C_{b_{c_k}}^n}\right)R_1\left(\left.\frac{\partial f}{\partial y_1}\right|_{z_{1_k},C_{b_{c_k}}^n}\right)^T\\&+\sigma^2\left(\left.\frac{\partial f}{\partial\theta_2}\right|_{z_{1_k},C_{b_{c_k}}^n}\right)\left(\left.\frac{\partial f}{\partial\theta_2}\right|_{z_{1_k},C_{b_{c_k}}^n}\right)^T\Bigg\}_{k=1}^N\Bigg)\end{aligned} \tag{12}$$

It is important to realize that the measurement equation (8) is linearized in the measurement error, and as a result, a linear regression is obtained. The linearization is justified as long as the measurement errors are small. The position measurement errors of a GPS receiver are indeed small: $\sigma_x=\sigma_y\approx5$ m, and σ_z is slightly larger; however, when baroaltitude measurements are used, σ_z is ≈3 m. Furthermore, the bearing-angle measurements provided by the camera are accurate: 5 mrad of angular error translate into a positional error of 5 m at a distance of 1000 m. It stands to reason that over the short measurement interval, the AHRS's random component of attitude-measurement errors is also small. We note a low-cost AHRS's systematic attitude-measurement errors: that is,

the bias θ_2, could be large. However, the functions that are being linearized are the trigonometric functions: because for the $\sin(\cdot)$ trigonometric function, the small-angle assumption holds up to ≈ 30 deg,

$$\frac{\pi}{6} \approx \sin\left(\frac{\pi}{6}\right) = \frac{1}{2}$$

and by the same token, the small-angle assumption is certainly valid up to 11 deg for the $\cos(\cdot)$ trigonometric function, we are confident that linearization is justified. Our key assumption is that the systematic attitude-measurement errors are constant over the short-measurement-time horizon. Hence, the parameter estimate is given by the solution of a linear regression and the parameter estimate is the maximum likelihood estimate. In other words, the parameter estimate is unbiased and the predicted covariance of the parameter estimation error is reliable. No iterations are required.

Let us denote the partial derivatives

$$\frac{\partial f}{\partial y_1}|_{z_1, C_b^n}$$

and

$$\frac{\partial f}{\partial \theta_2}|_{z_1, C_b^n}$$

with the 2×5 matrix

$$A \equiv \left.\frac{\partial f}{\partial y_1}\right|_{y_1, C_b^n} = \begin{bmatrix} 1 & 0 & a_{1,3} & a_{1,4} & a_{1,5} \\ 0 & 1 & a_{2,3} & a_{2,4} & a_{2,5} \end{bmatrix}$$

and the 2×3 matrix

$$B \equiv \left.\frac{\partial f}{\partial \theta_2}\right|_{z_1, C_b^n} = \begin{bmatrix} b_{1,1} & b_{1,2} & b_{1,3} \\ b_{2,1} & b_{2,2} & b_{2,3} \end{bmatrix}$$

The entries of the A and B matrices are evaluated using the measured variables z_1 and $C_{b_c}^n$. When variables measured at time k are used, the preceding matrices are denoted as A_k and B_k. Hence, the linear regression is explicitly given in Eq. (13),

$$\begin{pmatrix} f\left(z_{1_1}, C_{b_{c_1}}^n\right) \\ \cdot \\ \cdot \\ \cdot \\ f\left(z_{1_N}, C_{b_{c_N}}^n\right) \end{pmatrix} = \begin{bmatrix} I_2, & B_1 \\ \cdot & \cdot \\ \cdot & \cdot \\ \cdot & \cdot \\ I_2, & B_N \end{bmatrix} \theta + V \tag{13}$$

and the equation error covariance is

$$R = \operatorname{diag}\left(\left\{A_k R_1 A_k^T + \sigma^2 B_k B_k^T\right\}_{k=1}^N\right) \tag{14}$$

The solution of the linear regression, Eqs. (13) and (14), yields the closed-form formula for the minimum variance parameter estimate [10],

$$\hat{\theta} = \left[\sum_{k=1}^N \begin{bmatrix} I_2 \\ B_k^T \end{bmatrix} \left(A_k R_1 A_k^T + \sigma^2 B_k B_k^T\right)^{-1} [I_2, B_k]\right]^{-1} \times \sum_{k=1}^N \begin{bmatrix} I_2 \\ B_k^T \end{bmatrix} \left(A_k R_1 A_k^T + \sigma^2 B_k B_k^T\right)^{-1} f\left(z_{1_k}, C_{b_{c_k}}^n\right) \tag{15}$$

and the (predicted) parameter's estimation error covariance is

$$P \equiv E[(\theta - \hat{\theta})(\theta - \hat{\theta})^T] = \left[\sum_{k=1}^N \begin{bmatrix} I_2 \\ B_k^T \end{bmatrix} \left(A_k R_1 A_k^T + \sigma^2 B_k B_k^T\right)^{-1} (I_2, B_k)\right]^{-1} \tag{16}$$

Remark 1: Although the measurement equation is linearized, no iterations are required, and obtaining the parameter estimate and geolocating the target boils down to the solution of a linear regression, which entails the inversion of a 5×5 matrix, an easy computational task.

Remark 2: Because the parameter estimate is obtained via the solution of a linear regression, the parameter estimate is not biased; that is, the target is accurately geolocated. Moreover, a reliable data-driven estimate P of the localization error is also obtained.

A. Euler Angles' Estimation

The biases $\overline{\delta\phi}$, $\overline{\delta\theta}$, and $\overline{\delta\psi}$ in the Euler angles are not directly estimated; that is, the parameter

$$\theta_2 \neq \begin{pmatrix} \overline{\delta\phi} \\ \overline{\delta\theta} \\ \overline{\delta\psi} \end{pmatrix}$$

The errors in the Euler angles are obtained as follows. Denote with $\mathbf{v}\times \in \mathbb{R}^{3\times 3}$ the skew symmetric matrix associated with a generic vector $\mathbf{v} \equiv [\,v_1 \quad v_2 \quad v_3\,]^T \in \mathbb{R}^3$:

$$\mathbf{v}\times \triangleq \begin{bmatrix} 0 & -v_3 & v_2 \\ v_3 & 0 & -v_1 \\ -v_2 & v_1 & 0 \end{bmatrix}$$

We know [14] that

$$C_b^n \approx (I + \delta\boldsymbol{\Psi}\times) C_{b_c}^n$$

where

$$\delta\boldsymbol{\Psi} \equiv [\overline{\delta\alpha}, \overline{\delta\beta}, \overline{\delta\gamma}]^T \tag{17}$$

Hence, using the attitude-measurement bias estimate given in Eq. (15) (i.e., using the parameter estimate $\hat{\theta}_2$), the DCM estimate is obtained,

$$\hat{C}_b^n(t) = (I + \hat{\theta}_2\times) C_{b_c}^n(t), \qquad 0 \le t \le T_{\text{dwell}}$$

and the Euler angles' estimates $\hat{\psi}(t)$, $\hat{\theta}(t)$, and $\hat{\phi}(t)$ are obtained from the DCM $\hat{C}_b^n(t)$. T_{dwell} is the length of the measurement interval. The Euler angles' estimates and the DCM estimate $\hat{C}_b^n(t)$ can be used for $0 \le t \le T$, where $T > T_{\text{dwell}}$, provided that $T - T_{\text{dwell}}$ is sufficiently small. Now the raw IMU-calculated Euler angles ψ_c, θ_c, and ϕ_c are directly obtained from the DCM $C_{b_c}^n$ and vice versa. In conclusion, a method was devised for estimating the Euler angles from the IMU, provided raw Euler angles' measurements ψ_c, θ_c, and ϕ_c. Finally, the Euler angles' biases are calculated as follows. Let

$$\delta\psi_k := \psi_{c_k} - \hat{\psi}_k, \qquad \delta\theta_k := \theta_{c_k} - \hat{\theta}_k$$
$$\delta\phi_k := \phi_{c_k} - \hat{\phi}_k, \qquad k = 1, \ldots, N$$

where the subscript k indicates the variable value evaluated at instant time $k\Delta T$, with $\Delta T = T_{\text{dwell}}/N$. Finally, the estimates of the Euler angles' biases are

$$\hat{\overline{\delta\psi}} = \frac{1}{N}\sum_{k=1}^N \delta\psi_k, \qquad \hat{\overline{\delta\theta}} = \frac{1}{N}\sum_{k=1}^N \delta\theta_k, \qquad \hat{\overline{\delta\phi}} = \frac{1}{N}\sum_{k=1}^N \delta\phi_k$$

Having established the systematic Euler angles' measurement errors, when a one-shot bearing of a target is then taken at time $t > T_{\text{dwell}}$, the measured Euler angles are corrected as follows:

$$\hat{\psi}(t) := \psi_c(t) - \hat{\overline{\delta\psi}}, \qquad \hat{\theta}(t) := \theta_c(t) - \hat{\overline{\delta\theta}}$$
$$\hat{\phi}(t) := \phi_c(t) - \hat{\overline{\delta\phi}}, \qquad T_{\text{dwell}} < t$$

As a result, the target is rapidly and accurately geolocated.

B. Yaw-Angle Bias

During nonmaneuvering flight, the pitch and roll angles can be accurately measured using inclinometers (i.e., accelerometers). However, the yaw-angle measurement is somewhat problematic, and when a miniaturized magnetic flux gate and/or a compass are used, large measurement errors are recorded. The yaw-angle measurement error can be an order of magnitude higher than the pitch or roll angles' measurement errors; that is, the systematic pitch and roll measurement error are a couple of degrees, whereas the bias in the yaw-angle measurement can be more than 20 deg. Hence, to facilitate the estimation of the critical yaw-angle bias $\overline{\delta\psi}$, a reduced parameter vector θ_2 is employed; that is, during wing-level flight and constant speed, only the bias in the yaw-angle measurement is estimated,

$$\theta_2 = \overline{\delta\gamma}(\in R^1)$$

so that a reduced parameter vector comprising the three components x_P, y_P, and $\overline{\delta\gamma}$ is estimated.

The linear regression algorithm is modified as follows. The B matrices are 2×1 matrices:

$$B = \begin{pmatrix} b_{1,1} \\ b_{2,1} \end{pmatrix}$$

The entries $b_{1,1}$ and $b_{2,1}$ are computed as before. Note that $\overline{\delta\psi} \neq \overline{\delta\gamma}$; similar to the analysis in Sec. III.A, an estimate of the yaw-angle bias $\overline{\hat{\delta\psi}}$ must be obtained. If, however, the pitch and roll angles are small, $\overline{\delta\psi} \approx \overline{\delta\gamma}$.

Alternatively, because it is assumed that the pitch and roll angles are accurately measured and only the bias in the yaw angle is addressed, it is possible to derive the linear regression by perturbing the DCM in the yaw angle ψ and directly obtain the yaw-angle bias estimate $\overline{\hat{\delta\psi}}$.

The algorithm for the estimation of the yaw-angle measurement errors (i.e., the yaw-angle bias) is given in Sec. VI.

IV. Nonlinear Regression

The possibility of a large systematic attitude-measurement error (i.e., a large measurement bias θ_2) invalidates the small-angle assumption and, consequently, the linear hypothesis. We now acknowledge that the function f is nonlinear in the parameter θ_2. This forces us to address a nonlinear parameter estimation (i.e., nonlinear regression) problem. As before, the random measurement errors v_1 and v_2 are assumed small.

In the best tradition of the iterative least-squares (ILS) method for the solution of nonlinear regressions, assume that at iteration step i a good estimate $\hat{\theta}_2^{(i)}$ of the parameter θ_2 is available; in other words, the estimation error $\mid \hat{\theta}_2^{(i)} - \theta_2 \mid$ is small. The parameter θ_2 is associated with the DCM error δC_b^n, and $\hat{\theta}_2^{(i)}$ is associated with the DCM error $\delta\hat{C}_b^{n^{(i)}}$. The derivation of Eq. (9) is modified as follows. Write

$$f\left(z_1 - v_1, C_{b_c}^n - \delta C_b^n\right) = f\left[z_1 - v_1, C_{b_c}^n - \delta\hat{C}_b^{n^{(i)}} - \left(\delta C_b^n - \delta\hat{C}_b^{n^{(i)}}\right)\right]$$

For small v_1 and $\mid \delta\hat{C}_b^{n^{(i)}} - \delta C_b^n \mid$ (i.e., for small $\mid \hat{\theta}_2^{(i)} - \theta_2 \mid$), Taylor's theorem yields

$$\begin{aligned} &f\left[z_1 - v_1, C_{b_c}^n - \delta\hat{C}_b^{n^{(i)}} - \left(\delta C_b^n - \delta\hat{C}_b^{n^{(i)}}\right)\right] \\ &\quad \approx f\left(z_1, C_{b_c}^n - \delta\hat{C}_b^{n^{(i)}}\right) - \left.\frac{\partial f}{\partial y_1}\right|_{z_1, C_{b_c}^n - \delta\hat{C}_b^{n^{(i)}}} \cdot v_1 \\ &\quad - \left.\frac{\partial f}{\partial \theta_2}\right|_{z_1, C_{b_c}^n - \delta\hat{C}_b^{n^{(i)}}} \cdot v_2 - \left.\frac{\partial f}{\partial \theta_2}\right|_{z_1, C_{b_c}^n - \delta\hat{C}_b^{n^{(i)}}} \cdot \left(\theta_2 - \hat{\theta}_2^{(i)}\right) \end{aligned}$$

The linearized measurement equation is thus obtained

$$\begin{aligned} &f(z_1, C_{b_c}^n - \delta\hat{C}_b^{n^{(i)}}) + \left.\frac{\partial f}{\partial \theta_2}\right|_{z_1, C_{b_c}^n - \delta\hat{C}_b^{n^{(i)}}} \cdot \hat{\theta}_2^{(i)} \approx \theta_1 + \left.\frac{\partial f}{\partial \theta_2}\right|_{z_1, C_{b_c}^n - \delta\hat{C}_b^{n^{(i)}}} \cdot \theta_2 \\ &\quad + \left.\frac{\partial f}{\partial y_1}\right|_{z_1, C_{b_c}^n - \delta\hat{C}_b^{n^{(i)}}} \cdot v_1 + \left.\frac{\partial f}{\partial \theta_2}\right|_{z_1, C_{b_c}^n - \delta\hat{C}_b^{n^{(i)}}} \cdot v_2 \end{aligned}$$

Suppose $N(\geq 2)$ bearings are taken at the discrete time instants $k = 1, \ldots, N$ and the measurements

$$\left(z_{1_1}, C_{b_{c_1}}^n\right), \ldots, \left(z_{1_k}, C_{b_{c_k}}^n\right), \ldots, \left(z_{1_N}, C_{b_{c_N}}^n\right)$$

are accumulated. Using the linearized measurement equation, one generates the linear regression in the parameter $\theta \in R^5$, which is solved in the $i+1$ iteration:

$$\begin{aligned} &\begin{pmatrix} f\left(z_{1_1}, C_{b_{c_1}}^n - \delta\hat{C}_b^{n^{(i)}}\right) + \left.\frac{\partial f}{\partial \theta_2}\right|_{z_{1_1}, C_{b_{c_1}}^n - \delta\hat{C}_b^{n^{(i)}}} \cdot \hat{\theta}_2^{(i)} \\ \vdots \\ f\left(z_{1_N}, C_{b_{c_N}}^n - \delta\hat{C}_b^{n^{(i)}}\right) + \left.\frac{\partial f}{\partial \theta_2}\right|_{z_{1_N}, C_{b_{c_N}}^n - \delta\hat{C}_b^{n^{(i)}}} \cdot \hat{\theta}_2^{(i)} \end{pmatrix} \\ &= \begin{bmatrix} I_2 & \left.\frac{\partial f}{\partial \theta_2}\right|_{z_{1_1}, C_{b_{c_1}}^n - \delta\hat{C}_b^{n^{(i)}}} \\ \vdots & \vdots \\ I_2 & \left.\frac{\partial f}{\partial \theta_2}\right|_{z_{1_N}, C_{b_{c_N}}^n - \delta\hat{C}_b^{n^{(i)}}} \end{bmatrix} \theta + V \end{aligned} \tag{18}$$

The equation error

$$V \sim \mathbf{N}(0, R)$$

and, as before, its covariance is given by Eq. (12).

Set

$$C_b^n := C_{b_c}^n - \delta\hat{C}_b^{n^{(i)}}$$

and, as in Sec. III, proceed to evaluate the entries of the A and B matrices. The linear regression Eq. (18) is solved; that is, the $i+1$ iteration is performed and the new parameter estimates $\hat{\theta}_1$ and $\hat{\theta}_2^{(i+1)}$ are obtained.

To start the iteration, use the initial guess

$$\hat{\theta}_2^{(0)} = 0$$

When the attitude angles' measurement bias is less than 30 deg and the geometry is good, simulation experiments show that no more than five or six iterations are required.

At the conclusion of the iteration process, the positional-gyro bias estimate $\hat{\theta}_2$ and the predicted covariance P of the parameter estimation error are obtained. Finally, revisiting Eq. (8), an "improved" target position estimate might be calculated; that is,

$$\hat{\theta}_1 := \frac{1}{N}\sum_{k=1}^{N} f\left[z_{1_k}, (I + \hat{\theta}_2\times) C_{b_{c_k}}^n\right]$$

V. Two-Dimensional Geometry

The important scenario in which the MAV overflies the ground object is now considered. Thus, we confine our attention to the vertical planes x and z. We are interested in estimating the ground object's position x_P. Thus, the geolocation methodology developed in Secs. II and III is applied to the special 2-D case. The main equation for the 2-D case is obtained by setting $\phi = \psi = y = y_f = 0$ in Eq. (4). It is, however, instructive to rederive the main equation from first principles: in 2-D, the DCM

$$C_b^n = \begin{bmatrix} \cos\theta & \sin\theta \\ -\sin\theta & \cos\theta \end{bmatrix}$$

and Eq. (3) is reduced to

$$\begin{pmatrix} x_P \\ z_P \end{pmatrix} = \begin{pmatrix} x \\ z \end{pmatrix} + \frac{|R_{\text{LOS}}|}{\sqrt{x_f^2 + f^2}} \begin{bmatrix} \cos\theta & \sin\theta \\ -\sin\theta & \cos\theta \end{bmatrix} \begin{pmatrix} x_f \\ f \end{pmatrix} \tag{19}$$

The LOS angle is ζ, and thus

$$x_f = f\cot\zeta$$

Because

$$\frac{f}{\sqrt{x_f^2 + f^2}} = \sin\zeta$$

Eq. (19) gives

$$\begin{pmatrix} x_P \\ z_P \end{pmatrix} = \begin{pmatrix} x \\ z \end{pmatrix} + |R_{\text{LOS}}| \begin{bmatrix} \cos\theta & \sin\theta \\ -\sin\theta & \cos\theta \end{bmatrix} \begin{pmatrix} \cos\zeta \\ \sin\zeta \end{pmatrix} \tag{20}$$

The second equation in Eq. (20) yields

$$|R_{\text{LOS}}| = \frac{z - z_P}{\sin(\theta - \zeta)}$$

and inserting this expression into the first Eq. (20) yields *one* equation in x_P, referred to as the main equation, which relates the MAV's navigation state (x, z, θ), the position (x_P, z_P) of the ground object P, and the LOS measurements ζ:

$$x_P = x + (z - z_P)\cot(\theta - \zeta) \tag{21}$$

The actual measurements are

$$x_m = x + v_x, \quad v_x \sim \mathbf{N}\left(0, \sigma_x^2\right), \quad z_m = z + v_z$$
$$v_z \sim \mathbf{N}\left(0, \sigma_z^2\right), \quad \theta_m = \theta + b + v_\theta, \quad v_\theta \sim \mathbf{N}\left(0, \sigma_\theta^2\right)$$
$$\zeta_m = \zeta + v_\zeta, \quad v_\zeta \sim \mathbf{N}\left(0, \sigma_\zeta^2\right)$$

where the subscript m denotes measured variables and the bias b is the systematic measurement error of the MAV's pitch angle θ.

The ground object's position estimate is derived in Appendix A.I and is explicitly given by

$$\hat{x}_P = \frac{1}{d}\left[\sum_{k=1}^{N} \frac{(z_P - z_{m_k})^2}{\sigma_x^2\sin^4(\theta_{m_k} - \zeta_{m_k}) + \sigma_z^2\sin^2(\theta_{m_k} - \zeta_{m_k})\cos^2(\theta_{m_k} - \zeta_k) + (z_{m_k} - z_P)^2\left(\sigma_\theta^2 + \sigma_\zeta^2\right)}\right.$$
$$\cdot \sum_{k=1}^{N} \frac{(z_{m_k} - z_P)\cot(\theta_{m_k} - \zeta_{m_k}) + x_{m_k}}{\sigma_x^2 + \sigma_z^2\cot^2(\theta_{m_k} - \zeta_k) + \left(\dfrac{z_{m_k} - z_P}{\sin^2(\theta_{m_k} - \zeta_{m_k})}\right)^2\left(\sigma_\theta^2 + \sigma_\zeta^2\right)}$$
$$- \sum_{k=1}^{N} \frac{z_P - z_{m_k}}{\sigma_x^2\sin^2(\theta_{m_k} - \zeta_{m_k}) + \sigma_z^2\cos^2(\theta_{m_k} - \zeta_{m_k}) + \left(\dfrac{z_{m_k} - z_P}{\sin(\theta_{m_k} - \zeta_{m_k})}\right)^2\left(\sigma_\theta^2 + \sigma_\zeta^2\right)}$$
$$\left. \cdot \sum_{k=1}^{N} \frac{x_{m_k}(z_P - z_{m_k}) - (z_P - z_{m_k})^2\cot(\theta_{m_k} - \zeta_{m_k})}{\sigma_x^2\sin^2(\theta_{m_k} - \zeta_{m_k}) + \sigma_z^2\cos^2(\theta_{m_k} - \zeta_k) + \left(\dfrac{z_{m_k} - z_P}{\sin(\theta_{m_k} - \zeta_{m_k})}\right)^2\left(\sigma_\theta^2 + \sigma_\zeta^2\right)}\right]$$

and

$$\sigma_{x_P} = \sqrt{\frac{1}{d}\sum_{k=1}^{N} \frac{(z_P - z_{m_k})^2}{\sigma_x^2\sin^4(\theta_{m_k} - \zeta_{m_k}) + \sigma_z^2\sin^2(\theta_{m_k} - \zeta_{m_k})\cos^2(\theta_{m_k} - \zeta_{m_k}) + (z_{m_k} - z_P)^2\left(\sigma_\theta^2 + \sigma_\zeta^2\right)}} \tag{22}$$

where

$$d = \sum_{k=1}^{N} \frac{(z_P - z_{m_k})^2}{\sigma_x^2\sin^4(\theta_{m_k} - \zeta_{m_k}) + \sigma_z^2\sin^2(\theta_{m_k} - \zeta_{m_k})\cos^2(\theta_{m_k} - \zeta_k) + (z_{m_k} - z_P)^2\left(\sigma_\theta^2 + \sigma_\zeta^2\right)}$$
$$\cdot \sum_{k=1}^{N} \frac{1}{\sigma_x^2 + \sigma_z^2\cot^2(\theta_{m_k} - \zeta_k) + \left(\dfrac{z_{m_k} - z_P}{\sin^2(\theta_{m_k} - \zeta_{m_k})}\right)^2\left(\sigma_\theta^2 + \sigma_\zeta^2\right)}$$
$$- \left[\sum_{k=1}^{N} \frac{z_P - z_{m_k}}{\sigma_x^2\sin^2(\theta_{m_k} - \zeta_{m_k}) + \sigma_z^2\cos^2(\theta_{m_k} - \zeta_k) + \left(\dfrac{z_{m_k} - z_P}{\sin(\theta_{m_k} - \zeta_{m_k})}\right)^2\left(\sigma_\theta^2 + \sigma_\zeta^2\right)}\right]^2$$

When the pitch-angle measurement-error/bias b is large, an ILS algorithm may be employed to obtain a reliable estimate (see Appendix A.II and Sec. IV).

A. Optimal Geometry

Consider a constant-altitude h, constant speed V flyover. Set

$$\theta \equiv 0, \qquad z \equiv -h$$

$$\tan(\zeta_k) = \frac{h}{V\Delta T(N-k)}, \qquad k = 0, 1, \ldots, N$$

where N is the number of steps for which the object is detectable and, without loss of generality, assume $x_P = z_P = 0$.

The problem parameters are $V, h, x_P, z_P, \Delta T$, and N, and $\sigma_x, \sigma_z, \sigma_\theta$, and σ_{zeta}, To ascertain the impact of the geometry of the measurement arrangement on the accuracy of the geolocation of the ground object, one must first nondimensionalize/scale the variables and the parameters. We set

$$V \to V\frac{\Delta T}{h}, \qquad x_P \to \frac{x_P}{h}, \qquad z_P \to \frac{z_P}{h}$$

$$\sigma_x \to \frac{\sigma_x}{h}, \qquad \sigma_z \to \frac{\sigma_z}{h}, \qquad \sigma_{x_P} \to \frac{\sigma_{x_P}}{h}$$

The accuracy of the geolocation method is specified by σ_{x_P}. For the scenario under consideration, Eq. (22) yields

$$\sigma_{x_P} = \sqrt{\frac{1}{d}\sum_{k=1}^{N} \frac{1}{\sigma_x^2 \sin^4\zeta_{m_k} + \sigma_z^2 \sin^2\zeta_{m_k}\cos^2\zeta_{m_k} + \sigma_\theta^2 + \sigma_\zeta^2}} \tag{23}$$

where

$$d = \sum_{k=1}^{N} \frac{1}{\sigma_x^2 \sin^4\zeta_{m_k} + \sigma_z^2 \sin^2\zeta_{m_k}\cos^2\zeta_k + \sigma_\theta^2 + \sigma_\zeta^2} \cdot \sum_{k=1}^{N} \frac{\sin^4\zeta_{m_k}}{\sigma_x^2 \sin^4\zeta_{m_k} + \sigma_z^2 \sin^2\zeta_{m_k}\cos^2\zeta_k + \sigma_\theta^2 + \sigma_\zeta^2} - \left[\sum_{k=1}^{N} \frac{\sin^2\zeta_{m_k}}{\sigma_x^2 \sin^4\zeta_{m_k} + \sigma_z^2 \sin^2\zeta_{m_k}\cos^2\zeta_k + \sigma_\theta^2 + \sigma_\zeta^2}\right]^2 \tag{24}$$

and

$$\sin^2\zeta_{m_k} = \frac{1}{1 + (N-k)^2V^2} \tag{25}$$

Inserting Eq. (25) into Eqs. (23) and (24) yields

$$\sigma_{x_P} = \sqrt{\frac{1}{d}\sum_{k=1}^{N} \frac{[1 + (N-k)^2V^2]^2}{\sigma_x^2 + \sigma_z^2(N-k)^2V^2 + \left(\sigma_\theta^2 + \sigma_\zeta^2\right)\left[1 + (N-k)^2V^2\right]^2}}$$

and

$$d = \sum_{k=1}^{N} \frac{[1 + (N-k)^2V^2]^2}{\sigma_x^2 + \sigma_z^2(N-k)^2V^2 + \left(\sigma_\theta^2 + \sigma_\zeta^2\right)[1 + (N-k)^2V^2]^2} \cdot \sum_{k=1}^{N} \frac{1}{\sigma_x^2 + \sigma_z^2(N-k)^2V^2 + \left(\sigma_\theta^2 + \sigma_\zeta^2\right)[1 + (N-k)^2V^2]^2} - \left[\sum_{k=1}^{N} \frac{1 + (N-k)^2V^2}{\sigma_x^2 + \sigma_z^2(N-k)^2V^2 + \left(\sigma_\theta^2 + \sigma_\zeta^2\right)[1 + (N-k)^2V^2]^2}\right]^2$$

The nondimensional problem parameters are the measurement-error standard deviations σ_x, σ_z, σ_θ, σ_ζ, and V, which assumes the role of the V over h parameter in photogrammetry. Assuming $\sigma_x = \sigma_z = \sigma_\zeta = \sigma$ gives

$$\frac{\sigma_{x_P}}{\sigma} = \sqrt{\frac{1}{d}\sum_{k=1}^{N} \frac{[1 + (N-k)^2V^2]^2}{1 + (N-k)^2V^2 + \left(1 + \frac{\sigma_\theta^2}{\sigma^2}\right)[1 + (N-k)^2V^2]^2}} = \sqrt{\frac{1}{d}\sum_{k=1}^{N} \frac{1}{1 + \frac{\sigma_\theta^2}{\sigma^2} + \frac{1}{[1+(N-k)^2V^2]^2}}} \tag{26}$$

and

$$d = \sum_{k=1}^{N} \frac{[1 + (N-k)^2V^2]^2}{1 + (N-k)^2V^2 + \left(1 + \frac{\sigma_\theta^2}{\sigma^2}\right)[1 + (N-k)^2V^2]^2} \cdot \sum_{k=1}^{N} \frac{1}{1 + (N-k)^2V^2 + \left(1 + \frac{\sigma_\theta^2}{\sigma^2}\right)[1 + (N-k)^2V^2]^2} - \left[\sum_{k=1}^{N} \frac{1 + (N-k)^2V^2}{1 + (N-k)^2V^2 + \left(1 + \frac{\sigma_\theta^2}{\sigma^2}\right)[1 + (N-k)^2V^2]^2}\right]^2 \tag{27}$$

The impact of the geometry on the quality of the measurement is quantified by the ratio σ_{x_P}/σ. Hence, one must evaluate the sums in Eqs. (26) and (27).

VI. Algorithm Development for Three-Dimensional Geometry

As discussed in Sec. III.B, we consider the case in which the pitch and roll angles are accurately measured using inclinometers or accelerometers, but the yaw-angle measurement is affected by a systematic bias $\overline{\delta\psi}$. Hence, the scenario is now considered in which a MAV is moving in the three-dimensional space with bias only on the yaw-angle measurements. The target LOS is assumed measured by the azimuth and elevation angles ξ and ζ, as depicted in Fig. 1. Thus,

$$x_f = \sqrt{x_f^2 + y_f^2 + f^2}\cos(\zeta)\cos(\xi),$$

$$y_f = \sqrt{x_f^2 + y_f^2 + f^2}\cos(\zeta)\sin(\xi)$$

Because

$$\frac{f}{\sqrt{x_f^2 + y_f^2 + f^2}} = \sin\zeta$$

Eq. (4) becomes

$$\begin{pmatrix} x_P \\ y_P \end{pmatrix} = \begin{pmatrix} x \\ y \end{pmatrix} + \frac{z_P - z}{(0,0,1)C_b^n V_b} \cdot \begin{bmatrix} 1 & 0 & 0 \\ 0 & 1 & 0 \end{bmatrix} C_b^n V_b \tag{28}$$

where

$$V_b = \begin{bmatrix} \cos(\zeta)\cos(\xi) \\ \cos(\zeta)\sin(\xi) \\ \sin(\zeta) \end{bmatrix}$$

.

The following parameters are estimated:

$$\theta = [\theta_1, \theta_2]^T$$

where, as before,

$$\theta_1 = [x_P, y_P]^T$$

is the position of the ground object and now

$$\theta_2 = \overline{\delta\psi}$$

is the bias in the yaw measurement provided by the MAV's AHRS.

The measured variables are

$$y = [y_1, y_2]^T$$

where

$$y_1 = [x, y, z, \zeta, \xi, \theta, \phi]^T$$

and

$$y_2 = \psi$$

The measurements are

$$z_1 = y_1 + v_1, \qquad z_2 = \psi + \delta\psi + v_2$$

where $v_1 \in \mathbb{R}^7 \sim \mathcal{N}(0, R_{v_1})$ and $v_2 \in \mathbb{R} \sim \mathcal{N}(0, R_{v_2})$ are identically Gaussian noises.

Finally, the partial derivatives of the right-hand side of Eq. (28) are directly obtained as follows, to evaluate Eqs. (15) and (16) (see Appendix B):

$$A_k \equiv \left.\frac{\partial f}{\partial y_1}\right|_{z_{1_k}, z_{2_k}}$$

and

$$B_k \equiv \left.\frac{\partial f}{\partial y_2}\right|_{z_{1_k}, z_{2_k}}$$

VII. Simulation

A. Scenarios

Three scenarios relevant to the MAVs experimental setup [1] at the U.S. Air Force Research Laboratory (AFRL) are investigated (see Table 1). The MAV is equipped with a forward-looking and a side-looking camera with a horizontal/vertical field of view (FOV = 30 deg) and depression angle $\beta = 45$ deg. The scenarios refer to three maneuvers flown by AFRL's MAVs. The main difference among them is the dwell time T_{dwell} of the target inside the camera's footprint and hence the number of data samples available. The latter is determined by the footprint and the flown maneuver.

The MAV's airspeed is $V_a = 12.35$ m/s, its minimum turn radius is $R_{\min} \sim 60$ m, and the cruise altitude is 30 m $\leq h \leq$ 60 m. For each scenario, 100 Monte Carlo (MC) runs were performed and a statistical analysis is provided and summarized in Table 2. The rms error in target position estimate, the average predicted standard deviation $\bar{\sigma}_{\text{DGPS}}$ when differential GPS (DGPS) is used, the maximum error in estimated target position $[x_P, y_P]$, and the yaw-angle bias $\overline{\delta\psi}$ estimate are documented. For the target position $[x_P, y_P]$, we also provided the resulting average standard deviation $\bar{\sigma}_{\text{GPS}}$ when GPS is used.

1. Assumptions

Assumptions concerning the data acquisition process are as follows: constant-altitude flight is at $h = 45$ m, GPS data acquisition frequency is $f_{\text{GPS}} = 4$ Hz, $\sigma_\psi = \sigma_\theta = \sigma_\phi = 5$ deg, bias in the yaw-angle measurement is $\overline{\delta\psi} = 40$ deg, $\sigma_\zeta = \sigma_\xi = 0.5$ deg, DGPS horizontal uncertainty is $\sigma_x = \sigma_y \simeq 0.62$ m, $\sigma_z \simeq 1.5$ m, and GPS horizontal uncertainty is $\sigma_x = \sigma_y \simeq 5$ m.

Table 1 Scenarios considered in the simulation-based analysis

Maneuver	Employed camera
Overflight	Front
Flyby	Side
Loitering	Side

Table 2 Target geolocation:100 MC runs

		RMS	$\bar{\sigma}_{\text{DGPS}}$	Max error	$\bar{\sigma}_{\text{GPS}}$
Overflight	x, m	3.47	2.01	7.60	5.38
	y, m	4.39	3.96	10.93	6.37
	$\overline{\delta\psi}$, deg	5.45 deg	4.56 deg	13.03 deg	——
Flyby	x, m	20.28	8.77	45.62	10.10
	y, m	11.39	4.80	48.29	6.92
	$\overline{\delta\psi}$, deg	29.63 deg	12.04 deg	93.17 deg	——
Loitering	x, m	0.84	0.55	1.73	5.03
	y, m	1.12	0.48	2.2	5.02
	$\overline{\delta\psi}$, deg	0.34 deg	0.35 deg	0.8 deg	——

2. Overflight Using a Forward-Looking Camera

In this scenario, the MAV flies straight and level using a forward-looking camera pointed toward the object of interest. As shown in Fig. 2, the target image acquisition starts at a distance ρ_1 from the target and ends at a distance ρ_2, where

$$\rho_1 = \frac{h}{\tan(\pi/6)}, \qquad \rho_2 = \frac{h}{\tan(\pi/3)}$$

Hence, by expressing the dwell time of the object of interest inside the camera's footprint as a function of the altitude, one obtains

$$T_{\text{dwell}} = \frac{\rho_1 - \rho_2}{V_a} = \frac{h}{V_a}\left(\frac{1}{\tan(\pi/6)} - \frac{1}{\tan(\pi/3)}\right)$$
$$= \frac{2}{\sqrt{3}}\frac{h}{V_a} \simeq h \cdot 0.0935 \text{ [s/m]}$$

Typical trajectory and LOS angle measurements are shown in Fig. 3 and the simulation results of 100 MC runs are summarized in Table 2. The average condition number/ratio of eigenvalues of the nondimensional matrix P is $\simeq 30.8$, and the simulation time $T_{\text{dwell}} \simeq 4.2$ s; that is, $T_{\text{dwell}} \cdot f_{\text{GPS}} = 17$ data samples are available for each MC run.

3. Flyby Using the Side-Looking Camera

In this scenario, the MAV is flying straight and level while acquiring images of the object of interest from its side-looking camera. As shown in Fig. 4, target image acquisition starts at a distance ρ_1 before the target's projection onto the flight path of the MAV and ends at a distance ρ_2 after this point. To maintain the target in the center of the footprint, the offset L of the flight path from the target was chosen such that $L = h/\tan\beta$, and hence

$$\rho_1 = \rho_2 = \frac{h}{\sin\beta} \cdot \tan\left(\frac{\pi}{12}\right)$$

Furthermore, by expressing the dwell time of the target inside the footprint as a function of altitude, one obtains

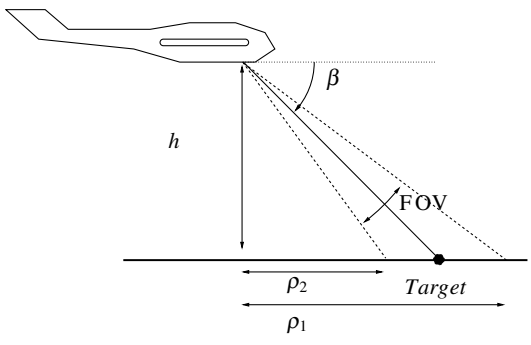

Fig. 2 Overflight flyover using the forward-looking camera.

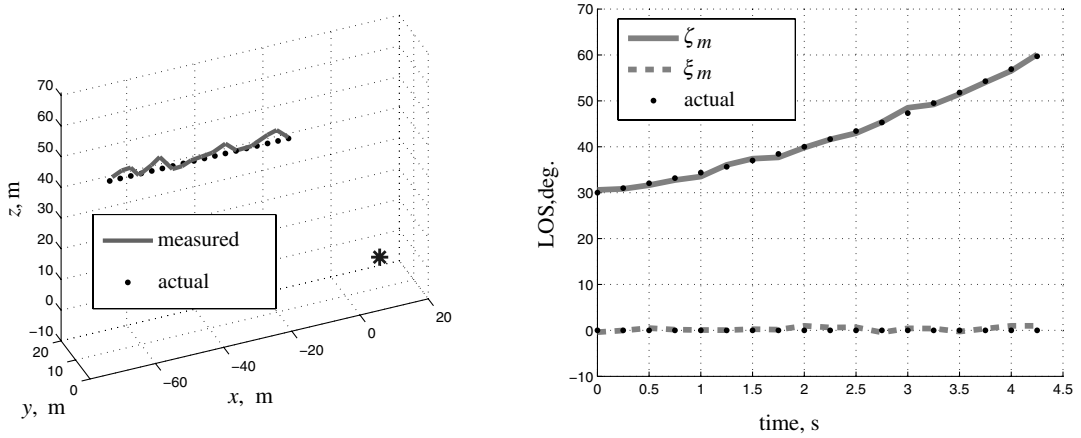

a) MAV's GPS measured positions **b) Target LOS angles**

Fig. 3 Overflight time histories.

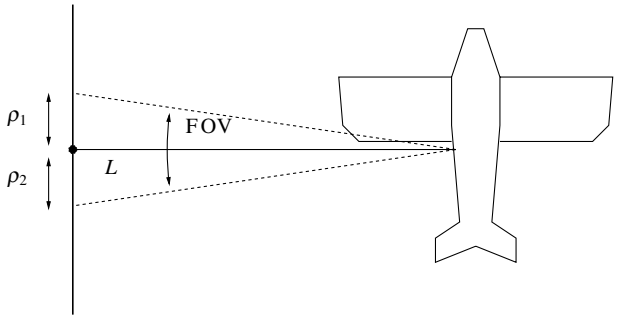

Fig. 4 Flyby with a side-looking camera.

$$T_{\text{dwell}} = \frac{\rho_1 + \rho_2}{V_a} = \frac{2h}{\sin\beta} \cdot \tan\left(\frac{\pi}{12}\right) \cdot \frac{1}{V_a} \simeq h \cdot 0.0614 \text{ s/m}$$

Typical trajectory and LOS angle measurements are shown in Fig. 3, and the results of 100 MC runs are summarized in Table 2. The average condition number (i.e., the ratio of the eigenvalues of the nondimensional matrix P) is $\simeq 93.8$. It is noticeably higher than in the case in which the forward-looking camera is used, mainly due to a reduced measurement interval $T_{\text{dwell}} \simeq 2.7$ s and, consequently, a reduced number of bearing samples $T_{\text{dwell}} \cdot f_{\text{GPS}} \simeq 11$.

4. Loitering Flight

In this scenario, the MAV is orbiting/loitering in the vicinity of the target while acquiring images of the target from its side-looking camera. One should pay attention to the nonlinear relation that holds between the altitude and the turn radius, to maintain the target inside the camera's footprint (see Fig. 6). Indeed, the bank angle ϕ plays an important role in defining the LOS in the body frame. It can be shown that at an altitude of $h \sim 60$ m, a ground target can be maintained inside the footprint, with turning radii in the range $\rho \in [60 \text{ m}, 120 \text{ m}]$ for camera depression angles:

$$\beta \in \left[\frac{\pi}{9}, \frac{\pi}{6}\right]$$

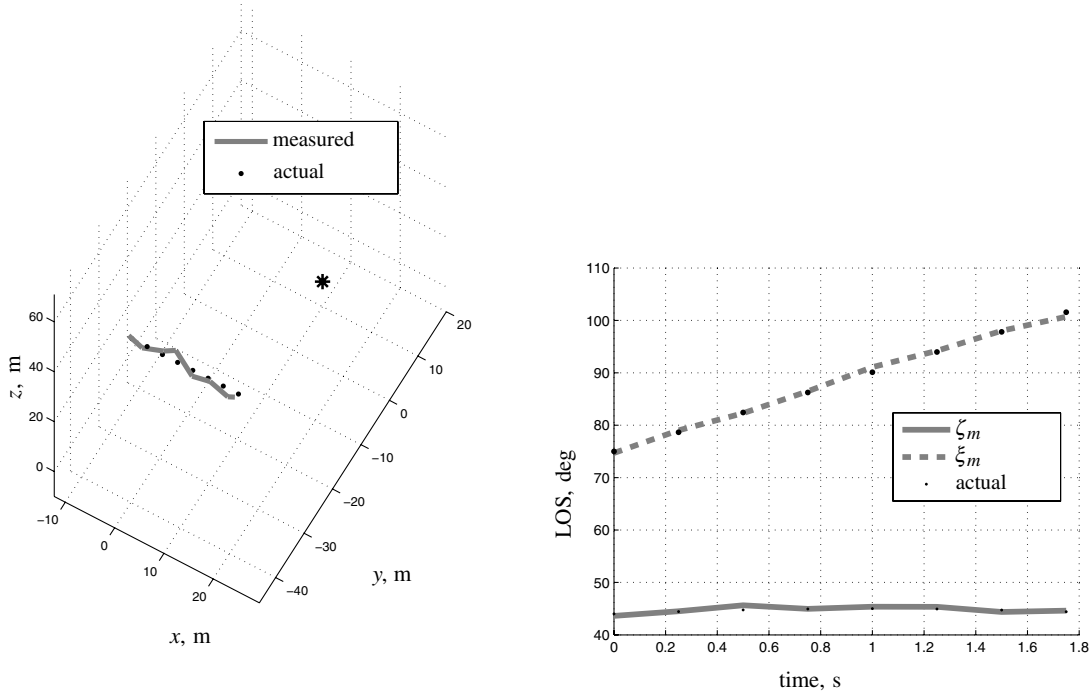

a) FB: MAV's GPS measured positions **b) FB: target LOS angles**

Fig. 5 Flyby time histories of GPS positions and LOS angles.

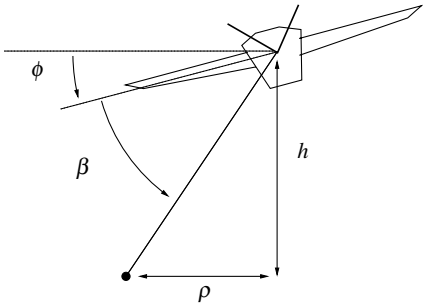

Fig. 6 Loitering/orbiting flight.

Note that when performing a loiter maneuver, the dwell time of the target inside the camera's footprint is not an issue because it does not depend on the footprint's geometry.

Typical trajectory and LOS angle measurements are shown in Fig. 7, and the results for 100 MC simulation runs are summarized in Table 2. The turn radius was set to $\rho \simeq 73$ m and the altitude $h = 45$ m, resulting in a bank angle of $\phi = 12$ deg. With the measurement interval extended to $T_{\text{dwell}} = 100$ s, $T_{\text{dwell}} \cdot f_{\text{GPS}} = 400$ bearing samples are processed, significantly reducing the average condition number of $P \sim 7.0$ compared with the previous two scenarios. Not only good estimates of target position and gyro bias were obtained, but most importantly, the experimentally resulting parameter-estimation error variances are consistent with the predicted parameter estimation error variances.

In the next section, the methods developed herein will be applied to the problem of one-shot target geolocalization, in which only one data point (i.e., only one camera frame featuring the object of interest) is available.

VIII. Single-Shot Geolocalization

We now consider geolocation using a single-shot measurement, as initiated by a mouse click of the operator. A point of interest $[x_T, y_T, z_T]^T$ of known elevation z_T is selected in the image and its bearing measurement $(\bar{\zeta}, \bar{\xi})$ is recorded. The true LOS is

$$\tilde{\zeta} \sim \mathcal{N}(\bar{\zeta}, \sigma_\zeta) \tilde{\xi} \sim \mathcal{N}(\bar{\xi}, \sigma_\xi)$$

We assume that using the technique presented in the previous sections, a current estimate of the bias $\overline{\delta\psi}$ in the yaw-angle measurement is already available, having been previously obtained as a result of tracking an arbitrary, but distinguishable, feature in the video stream: we refer to the tracking of an IP. Now the nonlinear relation between the point of interest and the vehicle state has the following form:

$$\begin{pmatrix} x_T \\ y_T \end{pmatrix} = \begin{pmatrix} x \\ y \end{pmatrix} + (z_T - z) \cdot \frac{1}{(0,0,1)C_b^n V_b} \begin{bmatrix} 1 & 0 & 0 \\ 0 & 1 & 0 \end{bmatrix} C_b^n V_b \quad (29)$$

The unscented transformation [15] is used to calculate the mean and covariance of the target position $[x_T, y_T]^T$. One rewrites Eq. (29) as

$$\mathbf{y} = h(\mathbf{x})$$

where $\mathbf{y} = [x_T, y_T]^T$ and

$$\mathbf{x} = [x, y, z, \psi, \theta, \phi, \overline{\delta\psi}, \zeta, \xi]^T$$

Denote the augmented state by $\mathcal{X} \in \mathbb{R}^{L \times 2L+1}$, where $L = 9$ is the state dimension, and where $\mathcal{X}_i$, the ith column of $\mathcal{X}$, is a sigma point. Initialize as follows:

$$\mathcal{X}_0 = \bar{\mathbf{x}} = (x_m, y_m, z_m, \psi_m, \theta_m, \xi_m, \tilde{\delta}_\psi, \tilde{\zeta}, \tilde{\xi}) \quad (30)$$

$$\mathcal{X}_i = \bar{\mathbf{x}} + \sqrt{(L+\lambda)P_{\mathbf{x}}} \qquad i = 1, \ldots, L \quad (31)$$

$$\mathcal{X}_i = \bar{\mathbf{x}} - \sqrt{(L+\lambda)P_{\mathbf{x}}} \qquad i = L+1, \ldots, 2L \quad (32)$$

where $\lambda = \alpha^2(L+k) - L$, with $\alpha = 10^{-3}$ and $k = 0$. The elements of $\bar{\mathbf{x}}$ and

$$P_{\mathbf{x}} = \text{diag}\left(\sigma_x^2, \sigma_y^2, \sigma_z^2, \sigma_\psi^2, \sigma_\theta^2, \sigma_\xi^2, \tilde{\sigma}^2_{\overline{\delta\psi}}, \sigma_\zeta^2, \sigma_{\dot{\xi}}^2\right)$$

are the measured values of the vehicle's state and the information on the measurement errors, respectively, with the exception of $\overline{\tilde{\delta\psi}}$ and $\tilde{\sigma}_{\overline{\delta\psi}}$, which are the yaw angle's bias mean and predicted estimation error variance.

Next, the following weights are defined:

$$W_0^m = \frac{\lambda}{L+\lambda}, \qquad W_0^c = \frac{\lambda}{L+\lambda} + (1 - \alpha^2 + \beta)$$
$$W_i^m = W_i^c = \frac{1}{2(L+\lambda)}$$

with $\beta = 2$. Denote with

$$\mathcal{Y}_i = h(\mathcal{X}_i) \quad (33)$$

the propagation of the sigma points through the nonlinear relation $h(\cdot)$. Finally, compute the predicted mean and variance for the random variable $\mathbf{y}$:

$$\bar{\mathbf{y}} \approx \sum_{i=0}^{2L} W_i^m \mathcal{Y}_i \quad (34)$$

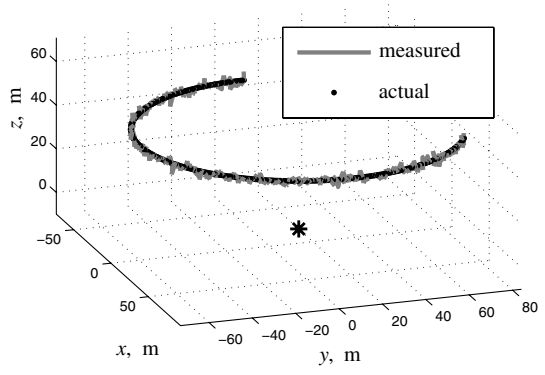

a) L: MAV's GPS measured positions

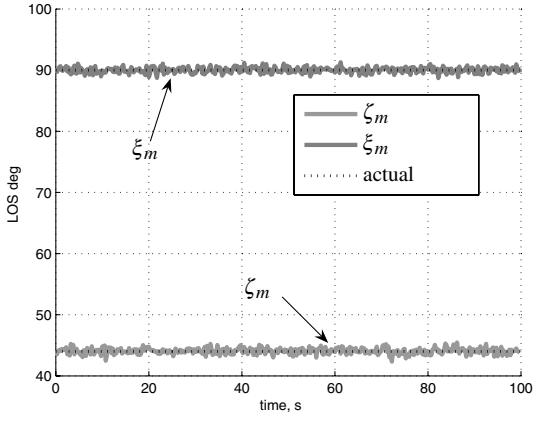

b) L: target LOS angles

Fig. 7 Loitering time histories of GPS positions and LOS angles.

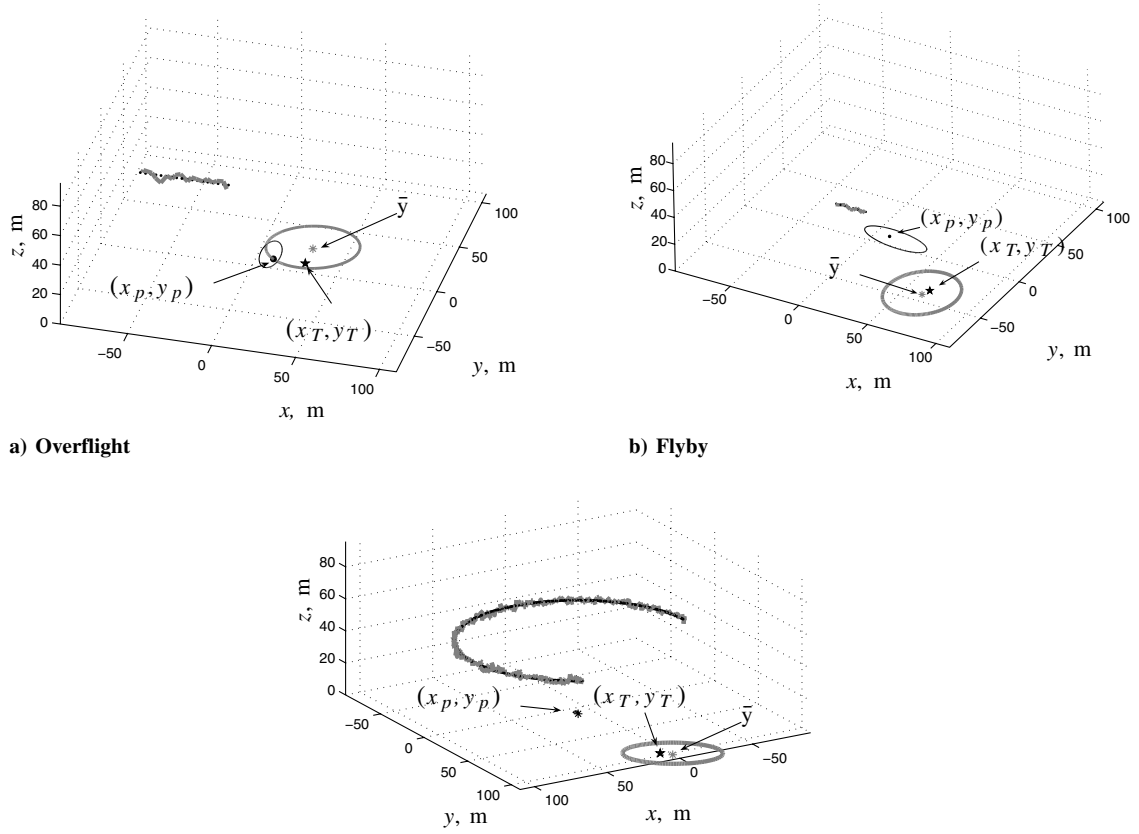

a) Overflight

b) Flyby

c) Loitering

Fig. 8 One-shot localization of a target's position for different approach scenarios.

$$P_{\mathbf{y}} \approx \sum_{i=0}^{2L} W_i^c (\mathcal{Y}_i - \bar{\mathbf{y}})(\mathcal{Y}_i - \bar{\mathbf{y}})' \tag{35}$$

Monte Carlo simulations were performed to evaluate the performance of the technique presented, with respect to the scenarios introduced in the previous section. Typical runs are presented in Fig. 8, in which the black star is the one-shot target's actual position (x_T, y_T), the asterisk is the expected mean value $\bar{\mathbf{y}}$, and the gray ellipse is the associated 99% confidence interval given by $P_{\mathbf{y}}$. The black dot and associated ellipse represent the result of the geolocalization of an arbitrary chosen point [the $IP \equiv (x_p, y_p)$] performed to estimate the bias $\overline{\delta\psi} = 40\,\text{deg}$ in the yaw-angle measurement. In Table 3, the statistical results are reported in terms of root mean square error (rms), average predicted variance $\bar{\sigma}_{\text{DGPS}}$, and maximum estimation error; the uncertainty associated with the GPS measurement errors $\bar{\sigma}_{\text{GPS}}$ is also listed.

The extensive simulations validate the one-shot geolocalization method developed in this paper. The achieved position uncertainty is about ± 10 m in the north and east directions. This level of performance was demonstrated in both overflight and loiter maneuvers, but with the exclusion of the flyby maneuver because of the extremely poor yaw bias estimate in that particular case. With the present values $\sigma_\psi = \sigma_\theta = \sigma_\phi = 5\,\text{deg}$, no benefit is gained by opting for a significantly longer loiter maneuver compared with a straight overflight.

Table 3 One-shot estimation performance:100 MC runs

		RMS, m	$\bar{\sigma}_{\text{DGPS}}$	Max error	$\bar{\sigma}_{\text{GPS}}$
Overflight	x, m	9.56	8.46	28.52	9.83
	y, m	7.73	6.92	21.55	8.53
Flyby	x, m	14.30	9.70	52.64	10.91
	y, m	25.94	11.21	71.64	12.27
Loitering	x, m	8.76	7.9	33.07	9.37
	y, m	6.97	6.55	25.83	8.24

IX. Flight Data Results

In this section, the approach previously presented is now validated using flight test data. The scenario is illustrated in Fig. 9. The MAV is flying a preplanned path in an urban environment with a cruise air speed of 12.35 m/s (∼24 kt). Two targets (white triangles) pop up in the video stream: they lie inside the camera footprint (black trapezoid). The human operator points them out by clicking on the two distinct video frames in the video stream in which the objects of interest are visible. It is required to accurately localize these targets on the area map.

In Fig. 9, the light path represents the GPS ground track. The arrows represent the heading as measured by the MAV's magnetic

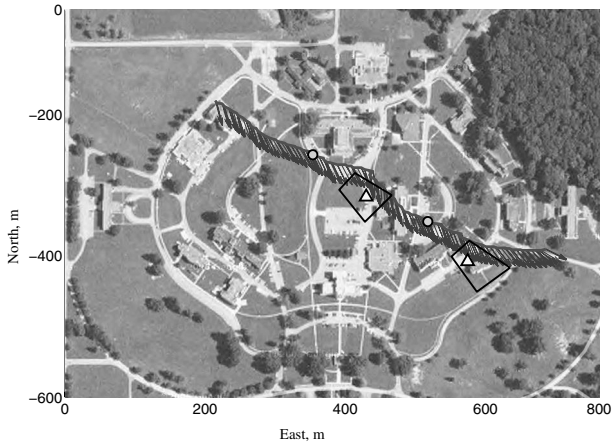

Fig. 9 Flight test: an urban scenario.

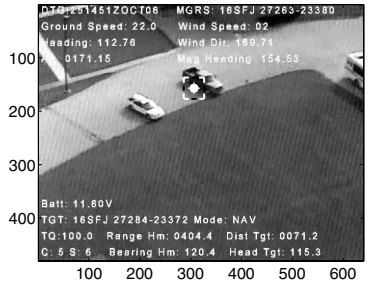

a) Designated target

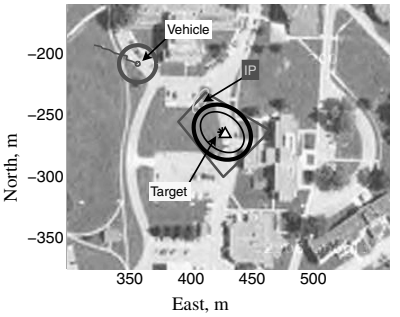

b) Localization results

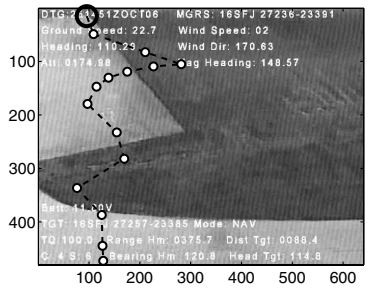

c) Tracked feature (IP): first frame

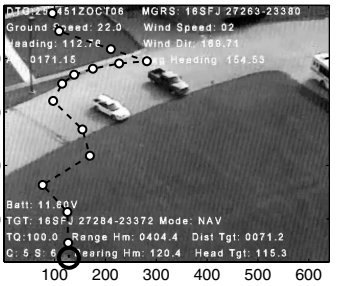

d) Tracked feature (IP): last frame

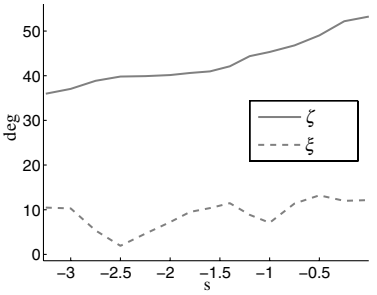

e) Azimuth and elevation of tracked feature

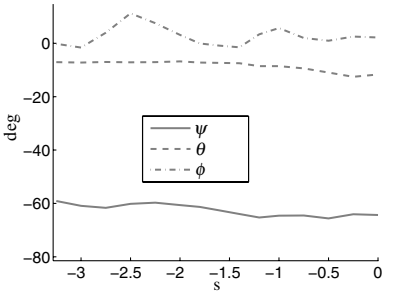

f) MAV Euler angles

Fig. 10 First target localization.

flux gate. The two gray dots are the MAV's GPS positions while acquiring the two frames in which the targets are pointed out. A wind of about 5 kt from the south was reported by an external weather station located on the roof of the highest building in the center of the urban area.

The following assumptions on the measurement process were employed: $\sigma_x = \sigma_y = 0.6$ m, $\sigma_z = 3$ m, $\sigma_\psi = \sigma_\theta = \sigma_\phi = 1$ deg, and $\sigma_\zeta = \sigma_\xi = 0.5$ deg.

The assumption of constant bias in the heading measurement provided by the flux gate is supported by Fig. 9, in which the arrows (the indicated heading measurements) display a significant, albeit constant, angular offset with respect to the direction of motion and which cannot be explained as a crab or sideslip angle.

In Figs. 10 and 11, the target localization results based on the actual flight data are reported. In particular, Figs. 10a and 11a refer to the frame in which the operator has pointed out the two pop-up targets. Once a target has been designated, a video clip before the frame in which the target was designated is chosen. A feature on the ground (an IP) is tracked using this video clip and the bias $\overline{\delta\psi}$ in the heading-angle measurement is estimated. Figures 10c, 10d, 11c, and 11d refer to IP tracking; the dashed line represents the path of the IP in the image plane. The resulting azimuth- and elevation-angle sequences are depicted in Figs. 10e and 11e. Figures 10f and 11f show the MAV's Euler angles during the duration of the video clip. Finally, Figs. 10b and 11b show the result of the complete localization process. The light path is the GPS ground track of the MAV during the video clip. The black dot and asterisk are the true position and estimated position of the tracked feature (the IP) during the yaw-angle sensor calibration. The white triangle and black asterisk are true position and estimated position of the unknown target. The thick and thin ellipsoids are the 99% respective confidence intervals when GPS or DGPS is used.

For the first target, a pickup truck in Fig. 10, the video clip selected is 3.25 s long so that 15 frames (i.e., 15 data points) are available. The tracked feature (the IP) is the top right corner of the pavement area in Fig. 10c. The operator has selected the target as it appears in the last frame. The resulting estimate of the bias in the yaw-angle measurement is

$$\hat{\overline{\delta\psi}} = -23.2\,\text{deg}, \qquad \sigma_{\overline{\delta\psi}} = 2.67\,\text{deg}$$

The square roots of the eigenvalues of the covariance matrix P_y of the target position estimation error, determined in part by the GPS uncertainty in the MAV's position, are

$$\sqrt{\lambda_1} \simeq 9.6\ \text{m}, \qquad \sqrt{\lambda_2} \simeq 8.4\ \text{m}$$

The resulting localization error, about $\sim$3 m, is practically insignificant.

For the second target, a sedan in Fig. 11, the video clip is 2.75 s long with 12 frames/data points available. The feature tracked in the video is a manhole in the middle of the street, behind the building in Fig. 11c. The operator has selected this IP, which appears in the first frame. The resulting yaw-angle bias estimate is

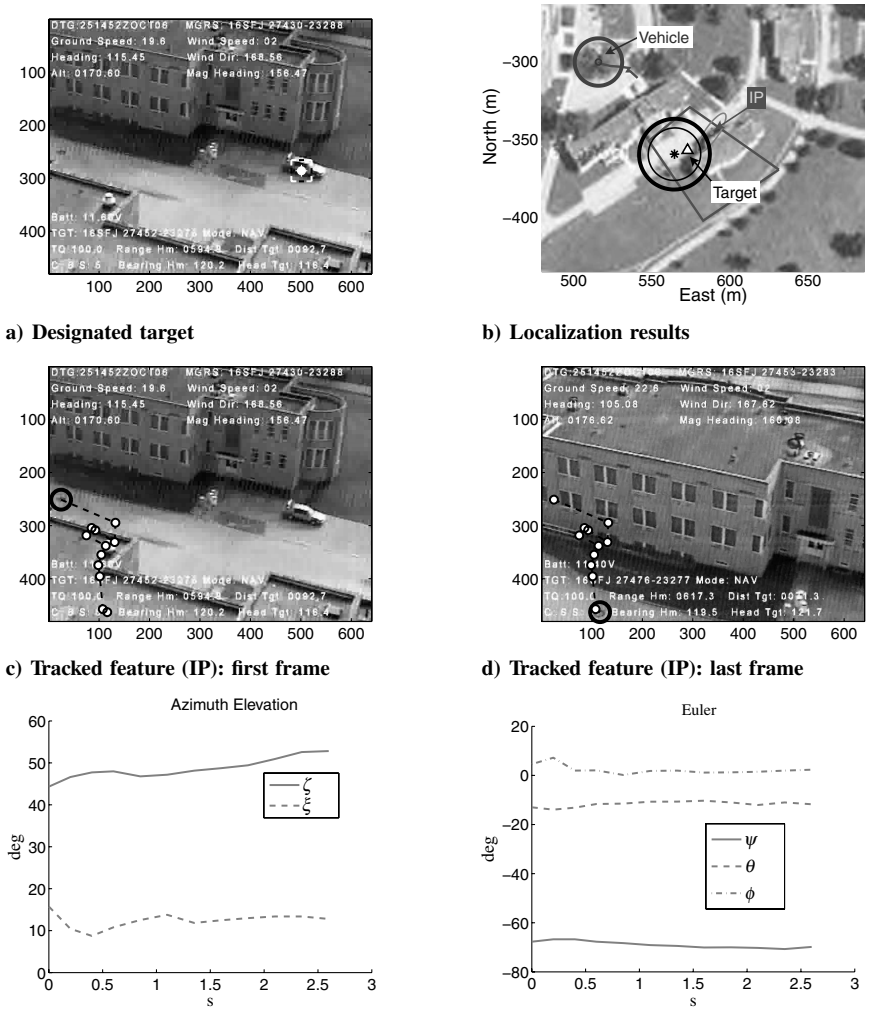

a) Designated target

b) Localization results

c) Tracked feature (IP): first frame

d) Tracked feature (IP): last frame

e) Azimuth and elevation of tracked feature

f) MAV Euler angles

Fig. 11 Second target localization.

$$\hat{\overline{\delta\psi}} = -21.2\,\text{deg}, \qquad \sigma_{\overline{\delta\psi}} = 3.91\,\text{deg}$$

The square root of the eigenvalues of the covariance $P_{\mathbf{y}}$ of the target position estimation error, using the GPS uncertainty in the vehicle position, is

$$\sqrt{\lambda_1} \simeq 8.9\ \text{m}, \qquad \sqrt{\lambda_2} \simeq 9.0\ \text{m}$$

The resulting localization error of ∼9.14 m is well inside the 99% confidence ellipse.

A. Cooperative Localization

In the case of multiple views of the same target, information fusion can be performed to reduce the uncertainty in the parameters' estimates. In particular, let us denote with $\mathbf{y}^i$ and $P_{\mathbf{y}}^i$ the target's position estimate and the associated covariance matrix as provided by vehicle i. Then fusing [16] the estimates gathered from several MAVs results in

$$\bar{\mathbf{y}} = \left[\sum_{i=1}^{n}\left(P_{\mathbf{y}}^i\right)^{-1}\right]^{-1} \cdot \sum_{i=1}^{n}\left(P_{\mathbf{y}}^i\right)^{-1}\mathbf{y}^i \tag{36}$$

$$P_{\mathbf{y}} = \left[\sum_{i=1}^{n}\left(P_{\mathbf{y}}^i\right)^{-1}\right]^{-1} \tag{37}$$

In Figs. 12 and 13 two examples are depicted. In both of them, the same target is asynchronously pointed out and localized by exploiting two different MAV video segments. This is the case of detection of a target from two different MAVs or detection of the same target in different segments of the same path of a single MAV. In both cases, the estimation of the target position can be carried out as illustrated in the previous sections and then the information can be fused as described in Eqs. (36) and (37). In the figures, black solid ellipses refer to the current uncertainties associated with the MAV position and localization of the target relative to MAV A; black dashed ellipses refer to MAV B; the thick bright ellipse and asterisk represent the resulting cooperative estimate of the target's position (white triangle). In particular, in Fig. 12, the target labeled as target 6 (a sedan) is asynchronously detected and localized by both MAV A and MAV B, and after the information is merged, the localization error is reduced to 5.30 m, whereas the eigenvalues of the matrix $P_{\mathbf{y}}$ are $\sqrt{\lambda_1} = 6.10$ m and $\sqrt{\lambda_2} = 5.77$ m (see Table 4). Similarly, in Fig. 13, the target labeled as target 9 (a pickup) is asynchronously detected and localized by two MAVs, as reported in Table 5. The final localization error is 15.60 m, whereas the eigenvalues of the matrix $P_{\mathbf{y}}$ are $\sqrt{\lambda_1} = 7.22$ m and $\sqrt{\lambda_2} = 5.82$ m. In both cases, the uncertainty reduction in terms of covariance matrix eigenvalues is remarkable.

Overall, the examples of this section show that the geolocation method developed in this paper is capable of accurately localizing unknown ground targets that pop up in the flight video stream and that a significant advantage in terms of localization uncertainty reduction can be obtained in the case of multiple views of the same target. Moreover, the flight data analysis has proved the technique

a) Vehicle A: target detection

b) Vehicle B: target detection

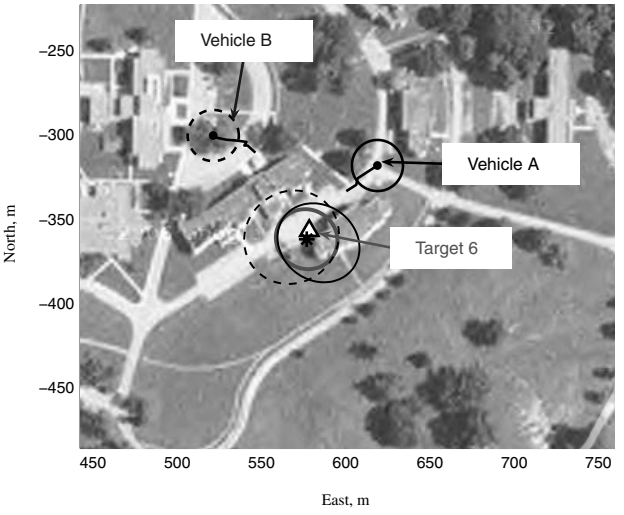

c) Cooperative localization

Fig. 12 Target 6.

a) Vehicle A: target detection

b) Vehicle B: target detection

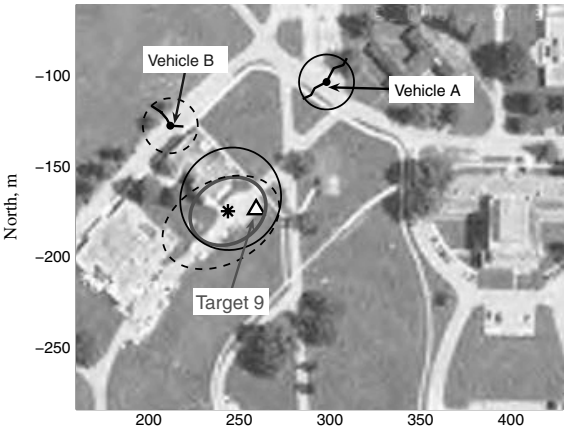

c) Cooperative localization

Fig. 13 Target 9.

Table 4 Localization results for target 6

	$\sqrt{\lambda_1}$, m	$\sqrt{\lambda_2}$, m	Error, m
MAV A	8.04	7.30	9.07
MAV B	9.49	8.90	11.23
Cooperative	6.10	5.77	5.30

Table 5 Localization results for target 9

	$\sqrt{\lambda_1}$, m	$\sqrt{\lambda_2}$, m	Error, m
MAV A	9.03	9.46	15.26
MAV B	11.31	7.56	20.72
Cooperative	7.22	5.82	15.60

developed in the paper to be fairly robust to poor knowledge about the noise characteristics. Indeed, in Sec. IX, actual flight test data are used with very limited information about the sensor's characteristics.

From a computational-load point of view, we should mention that, although the ILS version of the algorithm was used (Sec. IV) in all simulation and experimental results, convergence was obtained within an average of less than 10 iterations, hence proving that the proposed method is implementable for online applications.

X. Extensions

1) The use of baroaltitude measurements will further improve the target's localization accuracy. When the flight altitude $h = 100$ m, a calibrated baroaltitude measurement error with a variance of $\sigma_z = 3$ m is achievable.

2) The linear regression-algorithm-based geolocation method developed in this paper, which uses bearing measurements of a target taken over time, can easily be adapted to afford the tracking of moving targets. Similar to kinematic navigation, one stipulates the target's motion to be

$$x_P(t) = x_{P_0} + v_x t, \qquad y_P(t) = y_{P_0} + v_y t$$

where (x_{P_0}, y_{P_0}) is the target's initial position and v_x and v_y are the north and east components of the target's velocity, respectively. One now estimates the augmented parameter vector

$$\theta_1 := \begin{pmatrix} x_{P_0} \\ y_{P_0} \\ v_x \\ v_y \end{pmatrix}$$

Valid target position and velocity estimates will be obtained provided that the length of the estimation interval $N\Delta T$, where ΔT is the sampling interval, is sufficiently short compared with $1/\mathrm{BW}$, where BW is the target's maneuver bandwidth. This could prove to be a problem for MAVs if the target's velocity and maneuverability, compared with the MAVs, is high.

3) The novel geolocation methodology developed in this paper opens the door for on-the-fly gyro calibration: we refer to the AHRS's systematic attitude-measurement-error/bias estimation. Even better results will be achieved if bearings of a surveyed ground object IP are taken over time and the bias in the attitude measurement is exclusively estimated. In the parlance of INS [14], transfer alignment action is achieved.

XI. Conclusions

The localization accuracy of a ground object achieved when one bearing measurement is taken is generally poor, due primarily to the low quality of the attitude and heading reference systems onboard micro air vehicles. In this paper, a novel optical measurement system particularly suited to micro air vehicle operations is designed. The novel optical-measurement-based geolocation method hinges on feature tracking. The geolocation method developed in this paper yields a much-enhanced target localization accuracy.

The performance of geolocation using a camera and feature tracking was thoroughly investigated. We have shown that bearings measurements over time of a stationary ground object afford the accurate calculation of its location. With differential global positioning system horizontal-positioning accuracy of $\sim$0.2 m and bearing-angle accuracy of 0.5 deg, measurements taken during a $\sim$3-s overflight yield a target geolocation accuracy of $\sim$3 m. A byproduct of the novel optical geolocation method is the calibration of the air vehicle's attitude and heading reference systems; that is, the biases of the positional gyro are estimated. The error in the attitude measurement, averaged over the measurement interval, is estimated; that is, the gyros are calibrated. The main result of this paper is that the target's position and the micro air vehicle's systematic attitude-measurement errors can be jointly estimated using linear regression, provided that the random measurement errors are small (less than 2 deg) and the gyro's bias is less than 30 deg. As a result, the target is accurately geolocated. In addition, the geolocation method developed in this paper is capable of accurately localizing unknown ground targets that pop up in the flight video stream.

It is shown that good geolocation performance is achievable using a one-shot bearing measurement, provided that the attitude and heading reference systems is calibrated before reaching the target area using an initial point. Geolocation accuracy achieved using this method is $\sim$10 m. A significant advantage in terms of localization uncertainty reduction is realized in the case of multiple views of the same target, whether taken from the same vehicle or from a team of cooperating vehicles.

Appendix A: Two-Dimensional Geometry

The aim of this Appendix is to provide calculations to derive and implement algorithms and results presented in Sec. V, in which the scenario of MAV overflying the ground object is considered.

I. Target Geolocation

The main equation that relates the MAV's navigation state (x, z, θ), the position (x_P, z_P) of the ground object P, and the LOS measurements ζ, is given next:

$$x_P = x + (z - z_P)\cot(\theta - \zeta) \tag{A.1}$$

The actual measurements available are

$$x_m = x + v_x, \qquad v_x \sim \mathbf{N}\left(0, \sigma_x^2\right), \qquad z_m = z + v_z$$
$$v_z \sim \mathbf{N}\left(0, \sigma_z^2\right), \qquad \theta_m = \theta + b + v_\theta, \qquad v_\theta \sim \mathbf{N}\left(0, \sigma_\theta^2\right)$$
$$\zeta_m = \zeta + v_\zeta, \qquad v_\zeta \sim \mathbf{N}\left(0, \sigma_\zeta^2\right)$$

where the subscript m denotes measured variables and the bias b is the systematic measurement error of the MAV's pitch angle θ. Inserting these equations into the main equation (A.1) gives

$$\begin{aligned} x_P &= x_m - v_x + (z_m - v_z - z_P)\cot(\theta_m - b - v_\theta - \zeta_m + v_\zeta) \\ &\approx x_m - v_x - \cot(\theta_m - \zeta_m)v_z + (z_m - z_P)\Bigg[\cot(\theta_m - \zeta_m) \\ &\quad + \frac{1}{\sin^2(\theta_m - \zeta_m)}(b + v_\theta - v_\zeta)\Bigg] \end{aligned}$$

We have obtained the linear measurement equation in x_P and b:

$$\begin{aligned} (z_m - z_P)\cot(\theta_m - \zeta_m) + x_m &= x_P - \frac{z_m - z_P}{\sin^2(\theta_m - \zeta_m)}b \\ &\quad + v_x + \cot(\theta_m - \zeta_m)v_z - \frac{z_m - z_P}{\sin^2(\theta_m - \zeta_m)}(v_\theta - v_\zeta) \end{aligned}$$

Assume that $N(\geq 2)$ bearing measurements are taken and form the linear regression in the parameters x_P and b:

$$\begin{pmatrix} (z_{m_1}-z_P)\cot(\theta_{m_1}-\zeta_{m_1})+x_{m_1} \\ \vdots \\ (z_{m_N}-z_P)\cot(\theta_{m_N}-\zeta_{m_N})+x_{m_N} \end{pmatrix} = \begin{bmatrix} 1 & , & \frac{z_P-z_{m_1}}{\sin^2(\theta_{m_1}-\zeta_{m_1})} \\ \vdots & & \vdots \\ 1 & , & \frac{z_P-z_{m_N}}{\sin^2(\theta_{m_N}-\zeta_{m_N})} \end{bmatrix} \begin{pmatrix} x_P \\ b \end{pmatrix} + V \tag{A.2}$$

The covariance of the equation error V is

$$R = \operatorname{diag}\left(\left\{ \sigma_x^2 + \sigma_z^2\cot^2(\theta_{m_k}-\zeta_k) + \left(\frac{z_{m_k}-z_P}{\sin^2(\theta_{m_k}-\zeta_{m_k})}\right)^2(\sigma_\theta^2+\sigma_\zeta^2) \right\}_{k=1}^{N} \right) \tag{A.3}$$

The solution of the linear regression equations (A.2) and (A.3) yields the minimum variance parameter estimate:

$$\hat{\theta} = P \begin{pmatrix} \sum_{k=1}^{N} \frac{(z_{m_k}-z_P)\cot(\theta_{m_k}-\zeta_{m_k})+x_{m_k}}{\sigma_x^2+\sigma_z^2\cot^2(\theta_{m_k}-\zeta_k)+\left(\frac{z_{m_k}-z_P}{\sin^2(\theta_{m_k}-\zeta_{m_k})}\right)^2(\sigma_\theta^2+\sigma_\zeta^2)} \\ \sum_{k=1}^{N} \frac{x_{m_k}(z_P-z_{m_k})-(z_P-z_{m_k})^2\cot(\theta_{m_k}-\zeta_{m_k})}{\sigma_x^2\sin^2(\theta_{m_k}-\zeta_{m_k})+\sigma_z^2\cos^2(\theta_{m_k}-\zeta_k)+\left(\frac{z_{m_k}-z_P}{\sin(\theta_{m_k}-\zeta_{m_k})}\right)^2(\sigma_\theta^2+\sigma_\zeta^2)} \end{pmatrix} \tag{A.4}$$

where P is the parameter estimation error covariance and

$$P = \frac{1}{d}\begin{bmatrix} P_{1,1} & P_{1,2} \\ P_{1,2}^T & P_{2,2} \end{bmatrix}$$

with

$$P_{1,1} = \sum_{k=1}^{N} \frac{(z_P-z_{m_k})^2}{\sigma_x^2\sin^4(\theta_{m_k}-\zeta_{m_k}) + \sigma_z^2\sin^2(\theta_{m_k}-\zeta_{m_k})\cos^2(\theta_{m_k}-\zeta_k) + (z_{m_k}-z_P)^2\left(\sigma_\theta^2+\sigma_\zeta^2\right)}$$

$$P_{1,2} = -\sum_{k=1}^{N} \frac{z_P-z_{m_k}}{\sigma_x^2\sin^2(\theta_{m_k}-\zeta_{m_k}) + \sigma_z^2\cos^2(\theta_{m_k}-\zeta_k) + \left(\frac{z_{m_k}-z_P}{\sin(\theta_{m_k}-\zeta_{m_k})}\right)^2\left(\sigma_\theta^2+\sigma_\zeta^2\right)}$$

$$P_{2,2} = \sum_{k=1}^{N} \frac{1}{\sigma_x^2 + \sigma_z^2\cot^2(\theta_{m_k}-\zeta_k) + \left(\frac{z_{m_k}-z_P}{\sin^2(\theta_{m_k}-\zeta_{m_k})}\right)^2\left(\sigma_\theta^2+\sigma_\zeta^2\right)}$$

and the scalar

$$\begin{aligned} d = &\sum_{k=1}^{N} \frac{(z_P-z_{m_k})^2}{\sigma_x^2\sin^4(\theta_{m_k}-\zeta_{m_k}) + \sigma_z^2\sin^2(\theta_{m_k}-\zeta_{m_k})\cos^2(\theta_{m_k}-\zeta_k) + (z_{m_k}-z_P)^2\left(\sigma_\theta^2+\sigma_\zeta^2\right)} \\ &\cdot \sum_{k=1}^{N} \frac{1}{\sigma_x^2 + \sigma_z^2\cot^2(\theta_{m_k}-\zeta_k) + \left(\frac{z_{m_k}-z_P}{\sin^2(\theta_{m_k}-\zeta_{m_k})}\right)^2\left(\sigma_\theta^2+\sigma_\zeta^2\right)} \\ &- \left[\sum_{k=1}^{N} \frac{z_P-z_{m_k}}{\sigma_x^2\sin^2(\theta_{m_k}-\zeta_{m_k}) + \sigma_z^2\cos^2(\theta_{m_k}-\zeta_k) + \left(\frac{z_{m_k}-z_P}{\sin(\theta_{m_k}-\zeta_{m_k})}\right)^2\left(\sigma_\theta^2+\sigma_\zeta^2\right)} \right]^2 \end{aligned}$$

Hence, the ground object's position estimate is explicitly given by

$$\begin{aligned} \hat{x}_P = \frac{1}{d}\Bigg[&\sum_{k=1}^{N} \frac{(z_P-z_{m_k})^2}{\sigma_x^2\sin^4(\theta_{m_k}-\zeta_{m_k}) + \sigma_z^2\sin^2(\theta_{m_k}-\zeta_{m_k})\cos^2(\theta_{m_k}-\zeta_k) + (z_{m_k}-z_P)^2\left(\sigma_\theta^2+\sigma_\zeta^2\right)} \\ &\cdot \sum_{k=1}^{N} \frac{(z_{m_k}-z_P)\cot(\theta_{m_k}-\zeta_{m_k})+x_{m_k}}{\sigma_x^2 + \sigma_z^2\cot^2(\theta_{m_k}-\zeta_k) + \left(\frac{z_{m_k}-z_P}{\sin^2(\theta_{m_k}-\zeta_{m_k})}\right)^2\left(\sigma_\theta^2+\sigma_\zeta^2\right)} \\ &- \sum_{k=1}^{N} \frac{z_P-z_{m_k}}{\sigma_x^2\sin^2(\theta_{m_k}-\zeta_{m_k}) + \sigma_z^2\cos^2(\theta_{m_k}-\zeta_{m_k}) + \left(\frac{z_{m_k}-z_P}{\sin(\theta_{m_k}-\zeta_{m_k})}\right)^2\left(\sigma_\theta^2+\sigma_\zeta^2\right)} \\ &\cdot \sum_{k=1}^{N} \frac{x_{m_k}(z_P-z_{m_k})-(z_P-z_{m_k})^2\cot(\theta_{m_k}-\zeta_{m_k})}{\sigma_x^2\sin^2(\theta_{m_k}-\zeta_{m_k}) + \sigma_z^2\cos^2(\theta_{m_k}-\zeta_k) + \left(\frac{z_{m_k}-z_P}{\sin(\theta_{m_k}-\zeta_{m_k})}\right)^2\left(\sigma_\theta^2+\sigma_\zeta^2\right)} \Bigg] \end{aligned}$$

and

$$\sigma_{x_P} = \sqrt{\frac{1}{d}\sum_{k=1}^{N}\frac{(z_P - z_{m_k})^2}{\sigma_x^2\sin^4(\theta_{m_k}-\zeta_{m_k}) + \sigma_z^2\sin^2(\theta_{m_k}-\zeta_{m_k})\cos^2(\theta_{m_k}-\zeta_{m_k}) + (z_{m_k}-z_P)^2\left(\sigma_\theta^2+\sigma_\zeta^2\right)}} \tag{A.5}$$

II. Nonlinear Regression

When the pitch-angle measurement-error/bias b is large, use the ILS algorithm. The following iteration is performed:

$$\begin{pmatrix}\hat{x}_P^{(i+1)}\\ \hat{b}^{(i+1)}\end{pmatrix} = P^{(i)}\begin{pmatrix}\sum_{k=1}^{N}\frac{(z_{m_k}-z_P)\cot(\theta_{m_k}-\hat{b}^{(i)}-\zeta_{m_k})+x_{m_k}-\frac{z_{m_k}-z_P}{\sin^2(\theta_{m_k}-\hat{b}^{(i)}-\zeta_{m_k})}\hat{b}^{(i)}}{\sigma_x^2+\sigma_z^2\cot^2(\theta_{m_k}-\hat{b}^{(i)}-\zeta_{m_k})+\left(\frac{z_{m_k}-z_P}{\sin^2(\theta_{m_k}-\hat{b}^{(i)}-\zeta_{m_k})}\right)^2(\sigma_\theta^2+\sigma_\zeta^2)}\\ \sum_{k=1}^{N}\frac{x_{m_k}(z_P-z_{m_k})-(z_P-z_{m_k})^2\cot(\theta_{m_k}-\hat{b}^{(i)}-\zeta_{m_k})+\frac{(z_{m_k}-z_P)^2}{\sin^2(\theta_{m_k}-\hat{b}^{(i)}-\zeta_{m_k})}\hat{b}^{(i)}}{\sigma_x^2\sin^2(\theta_{m_k}-\hat{b}^{(i)}-\zeta_{m_k})-\sigma_z^2\cos^2(\theta_{m_k}-\hat{b}^{(i)}+\zeta_{m_k})+\left(\frac{z_{m_k}-z_P}{\sin(\theta_{m_k}-\hat{b}^{(i)}-\zeta_{m_k})}\right)^2(\sigma_\theta^2+\sigma_\zeta^2)}\end{pmatrix} \tag{A.6}$$

where $P^{(i)}$ is the parameter estimation error covariance and

$$P^{(i)} = \frac{1}{d^{(i)}}\begin{bmatrix}P_{1,1}^{(i)} & P_{1,2}^{(i)}\\ P_{1,2}^{(i)T} & P_{2,2}^{(i)}\end{bmatrix}$$

and where

$$P_{1,1}^{(i)} = \sum_{k=1}^{N}\frac{(z_P - z_{m_k})^2}{\sigma_x^2\sin^4(\theta_{m_k}-\hat{b}^{(i)}-\zeta_{m_k}) + \sigma_z^2\sin^2(\theta_{m_k}-\hat{b}^{(i)}-\zeta_{m_k})\cos^2(\theta_{m_k}-\hat{b}^{(i)}-\zeta_{m_k}) + (z_{m_k}-z_P)^2\left(\sigma_\theta^2+\sigma_\zeta^2\right)}$$

$$P_{1,2}^{(i)} = -\sum_{k=1}^{N}\frac{z_P - z_{m_k}}{\sigma_x^2\sin^2(\theta_{m_k}-\hat{b}^{(i)}-\zeta_{m_k}) + \sigma_z^2\cos^2(\theta_{m_k}-\hat{b}^{(i)}-\zeta_{m_k}) + \left(\frac{z_{m_k}-z_P}{\sin(\theta_{m_k}-\hat{b}^{(i)}-\zeta_{m_k})}\right)^2\left(\sigma_\theta^2+\sigma_\zeta^2\right)}$$

$$P_{2,2}^{(i)} = \sum_{k=1}^{N}\frac{1}{\sigma_x^2 + \sigma_z^2\cot^2(\theta_{m_k}-\hat{b}^{(i)}-\zeta_{m_k}) + \left(\frac{z_{m_k}-z_P}{\sin^2(\theta_{m_k}-\hat{b}^{(i)}-\zeta_{m_k})}\right)^2\left(\sigma_\theta^2+\sigma_\zeta^2\right)}$$

and the scalar

$$\begin{aligned}d^{(i)} = &\sum_{k=1}^{N}\frac{(z_P - z_{m_k})^2}{\sigma_x^2\sin^4(\theta_{m_k}-\hat{b}^{(i)}-\zeta_{m_k}) + \sigma_z^2\sin^2(\theta_{m_k}-\hat{b}^{(i)}-\zeta_{m_k})\cos^2(\theta_{m_k}-\hat{b}^{(i)}-\zeta_k) + (z_{m_k}-z_P)^2\left(\sigma_\theta^2+\sigma_\zeta^2\right)}\\ &\cdot\sum_{k=1}^{N}\frac{1}{\sigma_x^2 + \sigma_z^2\cot^2(\theta_{m_k}-\hat{b}^{(i)}-\zeta_{m_k}) + \left(\frac{z_{m_k}-z_P}{\sin^2(\theta_{m_k}-\hat{b}^{(i)}-\zeta_{m_k})}\right)^2\left(\sigma_\theta^2+\sigma_\zeta^2\right)}\\ &-\left[\sum_{k=1}^{N}\frac{z_P - z_{m_k}}{\sigma_x^2\sin^2(\theta_{m_k}-\hat{b}^{(i)}-\zeta_{m_k}) + \sigma_z^2\cos^2(\theta_{m_k}-\hat{b}^{(i)}-\zeta_k) + \left(\frac{z_{m_k}-z_P}{\sin(\theta_{m_k}-\hat{b}^{(i)}-\zeta_{m_k})}\right)^2\left(\sigma_\theta^2+\sigma_\zeta^2\right)}\right]^2\end{aligned}$$

The initial guess

$$\hat{b}^{(0)} = 0$$

Appendix B: A_k and B_k Matrix Calculations

The following is devoted to the computation of the matrices A_k and B_k in Eqs. (15) and (16), required for the implementation of the solution employed in both simulation (Secs. VII and VIII) and experimental (Sec. IX) scenarios, and presented in Sec. VI.

In particular we refer to the main equation:

$$\begin{pmatrix}x_P\\ y_P\end{pmatrix} = \begin{pmatrix}x\\ y\end{pmatrix} + \frac{z_P - z}{(0,0,1)C_b^nV_b}\cdot\begin{bmatrix}1 & 0 & 0\\ 0 & 1 & 0\end{bmatrix}C_b^nV_b \tag{B.1}$$

where

$$V_b = \begin{bmatrix} \cos(\zeta)\cos(\xi) \\ \cos(\zeta)\sin(\xi) \\ \sin(\zeta) \end{bmatrix}$$

The following parameters are estimated:

$$\theta_1 = [x_P, y_P]^T$$

is the position of the ground object, and

$$\theta_2 = \overline{\delta\psi}$$

is the bias in the yaw measurement provided by the MAV's AHRS.

The measured variables are

$$y_1 = [x, y, z, \zeta, \xi, \theta, \phi]^T$$

and

$$y_2 = \psi$$

By getting rid of the k subscript, the partial derivatives of the right-hand side of Eq. (B.1) are directly evaluated as follows:

$$A \equiv \left.\frac{\partial f}{\partial y_1}\right|_{z_1, z_2} = \begin{bmatrix} 1 & 0 & a_{1,3} & a_{1,4} & a_{1,5} & a_{1,6} & a_{1,7} \\ 0 & 1 & a_{2,3} & a_{2,4} & a_{2,5} & a_{1,6} & a_{1,7} \end{bmatrix}$$

We calculate

$$\frac{\partial V_b}{\partial \zeta} = \begin{bmatrix} -\sin(\zeta)\cos(\xi) \\ -\sin(\zeta)\sin(\xi) \\ \cos(\zeta) \end{bmatrix} \qquad \frac{\partial V_b}{\partial \xi} = \begin{bmatrix} -\cos(\zeta)\sin(\xi) \\ \cos(\zeta)\cos(\xi) \\ 0 \end{bmatrix}$$

and

$$a_{2,3} = -\frac{(0,1,0)C_b^n V_b}{(0,0,1)C_b^n V_b} \qquad a_{2,4} = (z_P - z)\frac{(0,1,0)C_b^n(\partial V_b/\partial\zeta)\cdot(0,0,1)C_b^n V_b - (0,1,0)C_b^n V_b \cdot (0,0,1)C_b^n(\partial V_b/\partial\zeta)}{\left[(0,0,1)C_b^n V_b\right]^2}$$

$$a_{2,5} = (z_P - z)\frac{(0,1,0)C_b^n(\partial V_b/\partial\xi)\cdot(0,0,1)C_b^n V_b - (0,1,0)C_b^n V_b \cdot (0,0,1)C_b^n(\partial V_b/\partial\xi)}{\left[(0,0,1)C_b^n V_b\right]^2}$$

$$a_{2,6} = (z_P - z)\frac{(0,1,0)(\partial C_b^n/\partial\theta)V_b\cdot(0,0,1)C_b^n V_b - (0,1,0)C_b^n V_b \cdot (0,0,1)(\partial C_b^n/\partial\theta)V_b}{\left[(0,0,1)C_b^n V_b\right]^2}$$

$$a_{2,7} = (z_P - z)\frac{(0,1,0)(\partial C_b^n/\partial\phi)V_b\cdot(0,0,1)C_b^n V_b - (0,1,0)C_b^n V_b \cdot (0,0,1)(\partial C_b^n/\partial\phi)V_b}{\left[(0,0,1)C_b^n V_b\right]^2}$$

$$\frac{\partial C_b^n}{\partial\psi} = \begin{bmatrix} -\sin(\psi)\cos(\theta) & -\sin(\psi)\sin(\theta)\sin(\phi) - \cos(\psi)\cos(\phi) & \cos(\psi)\sin(\phi) - \sin(\psi)\sin(\theta)\cos(\phi) \\ \cos(\psi)\cos(\theta) & -\sin(\psi)\cos(\phi) + \cos(\psi)\sin(\theta)\sin(\phi) & \cos(\psi)\sin(\theta)\cos(\phi) + \sin(\psi)\sin(\phi) \\ 0 & 0 & 0 \end{bmatrix}$$

$$\frac{\partial C_b^n}{\partial\theta} = \begin{bmatrix} -\cos(\psi)\sin(\theta) & \cos(\psi)\cos(\theta)\sin(\phi) & \cos(\psi)\cos(\theta)\cos(\phi) \\ -\sin(\psi)\sin(\theta) & \sin(\psi)\cos(\theta)\sin(\phi) & \sin(\psi)\cos(\theta)\cos(\phi) \\ -\cos(\theta) & -\sin(\theta)\sin(\phi) & -\sin(\theta)\cos(\phi) \end{bmatrix}$$

$$\frac{\partial C_b^n}{\partial\phi} = \begin{bmatrix} 0 & \cos(\psi)\sin(\theta)\cos(\phi) + \sin(\psi)\sin(\phi) & \sin(\psi)\cos(\phi) - \cos(\psi)\sin(\theta)\sin(\phi) \\ 0 & -\cos(\psi)\sin(\phi) + \sin(\psi)\sin(\theta)\cos(\phi) & -\sin(\psi)\sin(\theta)\sin(\phi) - \cos(\psi)\cos(\phi) \\ 0 & \cos(\theta)\cos(\phi) & -\cos(\theta)\sin(\phi) \end{bmatrix}$$

$$a_{1,3} = -\frac{(1,0,0)C_b^n V_b}{(0,0,1)C_b^n V_b}$$

$$a_{1,4} = (z_P - z)\frac{(1,0,0)C_b^n(\partial V_b/\partial\zeta)\cdot(0,0,1)C_b^n V_b - (1,0,0)C_b^n V_b \cdot (0,0,1)C_b^n(\partial V_b/\partial\zeta)}{\left[(0,0,1)C_b^n V_b\right]^2}$$

$$a_{1,5} = (z_P - z)\frac{(1,0,0)C_b^n(\partial V_b/\partial\xi)\cdot(0,0,1)C_b^n V_b - (1,0,0)C_b^n V_b \cdot (0,0,1)C_b^n(\partial V_b/\partial\xi)}{\left[(0,0,1)C_b^n V_b\right]^2}$$

$$a_{1,6} = (z_P - z)\frac{(1,0,0)\left(\partial C_b^n/\partial\theta\right)V_b\cdot(0,0,1)C_b^n V_b - (1,0,0)C_b^n V_b \cdot (0,0,1)\left(\partial C_b^n/\partial\theta\right)V_b}{[(0,0,1)C_b^n V_b]^2}$$

$$a_{1,7} = (z_P - z)\frac{(1,0,0)\left(\partial C_b^n/\partial\phi\right)V_b\cdot(0,0,1)C_b^n V_b - (1,0,0)C_b^n V_b \cdot (0,0,1)\left(\partial C_b^n/\partial\phi\right)V_b}{\left[(0,0,1)C_b^n V_b\right]^2}$$

Moreover,

$$B \equiv \left.\frac{\partial f}{\partial y_2}\right|_{z_1,z_2} = \begin{bmatrix} b_{1,1} \\ b_{2,1} \end{bmatrix}$$

with

$$b_{1,1} = \frac{z_P - z}{\left[(0,0,1)C_b^n V_b\right]} \cdot (1,0,0)\frac{\partial C_b^n}{\partial \psi} V_b$$

$$b_{2,1} = \frac{z_P - z}{\left[(0,0,1)C_b^n V_b\right]} \cdot (0,1,0)\frac{\partial C_b^n}{\partial \psi} V_b$$

Acknowledgment

The views expressed in this article are those of the authors and do not reflect the official policy or position of the U.S. Air Force, U.S. Department of Defense, or U.S. Government. The research was performed while N. Ceccarelli held a National Research Council Research Associateship Award at the U.S. Air Force Research Laboratory, Air Vehicles Directorate.

References

[1] Gross, D., Rasmussen, S., Chandler, P., and Feitshans, G., "Cooperative Operations in Urban Terrain (COUNTER)," *Defense Transformation and Network-Centric Systems*, Proceedings of SPIE, Vol. 5820, SPIE—the International Society for Optical Engineering, Bellingham, WA, Mar. 2005

[2] "Unmanned Aerial Systems Roadmap 2005–2030," Office of the Secretary of Defense, TR DC 20301, Washington, D.C., Aug. 2005.

[3] Ludington, B., Johnson, E., and Vachtsevanos, G., "Augmenting UAV Autonomy," *IEEE Robotics and Automation Magazine*, Vol. 13, No. 3, Sept. 2006, pp. 63–71. doi:10.1109/MRA.2006.1678140

[4] Barber, D. B., Redding, J. D., Mclain, T. W., Beard, R. W., and Taylor, C. N., "Vision-Based Target Geolocation Using a Fixed-Wing Miniature Air Vehicle," *Journal of Intelligent and Robotic Systems: Theory and Applications*, Vol. 47, No. 4, Dec. 2006, pp. 361–382. doi:10.1007/s10846-006-9088-7

[5] Campbell, M. E., and Wheeler, M., "A Vision Based Geolocation Tracking System for UAVs," AIAA Guidance, Navigation, and Control Conference and Exhibit, Keystone, CO, AIAA Paper 2006-6246, 21–24 Aug. 2006.

[6] Lowe, D. G., "Distinctive Image Features from Scale-Invariant Keypoints," *International Journal of Computer Vision*, Vol. 60, No. 2, 2004, pp. 91–110. doi:10.1023/B:VISI.0000029664.99615.94

[7] Webb, T. P., Prazenica, R. J., Kurdila, A. J., and Lind, R., "Vision-Based State Estimation for Autonomous Micro Air Vehicles," AIAA Guidance, Navigation, Control Conference and Exhibit Providence, RI, AIAA Paper 2004-5349, 16–19 Aug. 2004.

[8] Kehoe, J. J., Causey, R. S., Abdulrahim, M., and Lindx, R., "Waypoint Navigation for a Micro Air Vehicle Using Vision-Based Attitude Estimation," AIAA Guidance, Navigation, and Control Conference and Exhibit, San Francisco, AIAA Paper 2005-6400, 15–18 Aug. 2005.

[9] Koch, A., Wittich, H., and Thielecke, F., "A Vision-Based Navigation Algorithm for a VTOL-UAV," AIAA Guidance, Navigation, and Control Conference and Exhibit, Keystone, CO, AIAA Paper 2006-6546, 21–24 Aug. 2006.

[10] Draper, N. R., and Smith, H., *Applied Regression Analysis*, Wiley-Interscience, New York, 1998, pp. 108–111.

[11] Veth, M. J., "Optical and Inertial Sensor Fusion," Ph.D. Dissertation, U.S. Air Force Inst. of Technology, Wright–Patterson AFB, OH, Sept. 2006.

[12] Pachter, M., Ceccarelli, N., and Chandler, P. R., "Vision-Based Target Geolocation Using Feature Tracking," AIAA Guidance, Navigation and Control Conference and Exhibit, Hilton Head, SC, AIAA Paper 2007-6863, 20–23 Aug. 2007.

[13] Pachter, M., Ceccarelli, N., and Chandler, P. R., "Vision-Based Target Geolocation Using Camera Equipped MAVs," *2007 IEEE Conference on Decision and Control* (to be published).

[14] Titterton, D., and Weston, J., *Strapdown Inertial Navigation Technology*, 2nd ed., IEE Radar, Sonar and Navigation Series, Vol. 17, Peter Peregrinus, London, for Inst. of Electrical Engineers, London, 2005, pp. 342–347.

[15] Julier, S. J., "The Scaled Unscented Transformation," *Proceedings of the 2002 American Control Conference*, Vol. 6, Inst. of Electronics and Electrical Engineers, Piscataway, NJ, 6 May 2002, pp. 4555–4559.

[16] Bar-Shalom, Y., and Li, X.-R., *Multitarget–Multisensor Tracking: Principles and Techniques*, YBS Publishing, Storrs, CT, Sept. 1995, p. 429.